Journal of Neuroinflammation

RESEARCH

Open Access

Prolactin deficiency drives diabetes-associated cognitive dysfunction by inducing microglia-mediated synaptic loss

Jiaxuan Jiang[1,2†], Pengzi Zhang[1,2†], Yue Yuan[1,2†], Xiang Xu[1,2], Tianyu Wu[1,2], Zhou Zhang[1,2*], Jin Wang[1,2*] and Yan Bi[1,2*]

Abstract

Background Diabetes-associated cognitive dysfunction, characterized by hippocampal synaptic loss as an early pathological feature, seriously threatens patients' quality of life. Synapses are dynamic structures, and hormones play important roles in modulating the formation and elimination of synapses. The pituitary, the master gland of the body, releases several hormones with multiple roles in hippocampal synaptic regulation. In this study, we aimed to explore the relationship between pituitary hormones and cognitive decline in diabetes.

Methods A total of 744 patients with type 2 diabetes (T2DM) (445 men and 299 postmenopausal women) who underwent serum pituitary hormone level assessments, comprehensive cognitive evaluations and MRI scans were enrolled. Dynamic diet interventions were applied in both chow diet-fed mice and high-fat diet (HFD)-fed diabetic mice. The cognitive performance and hippocampal pathology of prolactin (PRL)-knockout mice, neuronal prolactin receptor (PRLR)-specific knockout mice and microglial PRLR-specific knockout mice were assessed. Microglial PRLR-specific knockout mice were fed an HFD to model diabetes. Diabetic mice received an intracerebroventricular infusion of recombinant PRL protein or vehicle.

Results This clinical study revealed that decreased PRL levels were associated with cognitive impairment and hippocampal damage in T2DM patients. In diabetic mice, PRL levels diminished before hippocampal synaptic loss and cognitive decline occurred. PRL loss could directly cause cognitive dysfunction and decreased hippocampal synaptic density. Knockout of PRLR in microglia, rather than neurons, induced hippocampal synaptic loss and cognitive impairment. Furthermore, blockade of PRL/PRLR signaling in microglia exacerbated abnormal microglial phagocytosis of synapses, further aggravating hippocampal synaptic loss and cognitive impairment in diabetic mice. Moreover, PRL infusion reduced microglia-mediated synaptic loss, thereby alleviating cognitive impairment in diabetic mice.

†Jiaxuan Jiang, Pengzi Zhang and Yue Yuan contributed equally to this work.

*Correspondence:
Zhou Zhang
zhangzhou@smail.nju.edu.cn
Jin Wang
wangjin@smail.nju.edu.cn
Yan Bi
biyan@nju.edu.cn

Full list of author information is available at the end of the article

© The Author(s) 2024. **Open Access** This article is licensed under a Creative Commons Attribution-NonCommercial-NoDerivatives 4.0 International License, which permits any non-commercial use, sharing, distribution and reproduction in any medium or format, as long as you give appropriate credit to the original author(s) and the source, provide a link to the Creative Commons licence, and indicate if you modified the licensed material. You do not have permission under this licence to share adapted material derived from this article or parts of it. The images or other third party material in this article are included in the article's Creative Commons licence, unless indicated otherwise in a credit line to the material. If material is not included in the article's Creative Commons licence and your intended use is not permitted by statutory regulation or exceeds the permitted use, you will need to obtain permission directly from the copyright holder. To view a copy of this licence, visit http://creativecommons.org/licenses/by-nc-nd/4.0/.

Conclusion PRL is associated with cognitive dysfunction and hippocampal damage in T2DM patients. In diabetes, a decrease in PRL level drives hippocampal synaptic loss and cognitive impairment by increasing microglia-mediated synapse engulfment. Restoration of PRL levels ameliorates cognitive dysfunction and hippocampal synaptic loss in diabetic mice.

Keywords Prolactin, Diabetes mellitus, Cognitive dysfunction, Microglia, Phagocytosis, Synapses

Introduction

Type 2 diabetes mellitus (T2DM) is the most common chronic metabolic disease and causes varying degrees of damage to all vital organs of the body. The epidemic of T2DM and its complications presents a major global health threat [1, 2]. Cognitive dysfunction has drawn increasing attention as an important complication of diabetes. Diabetes-associated cognitive dysfunction can be roughly divided into three different stages according to disease progression: diabetes-associated cognitive function decrements, mild cognitive impairment (MCI) and dementia [3]. Dementia, an advanced diabetes-associated cognitive dysfunction, is the second leading cause of death in patients with diabetes [4]. Current methods for managing the cognitive impairment of individuals with diabetes rely on glycemic control, dietary and lifestyle interventions, and neurotrophic therapy. However, clinical trials have shown that the beneficial effects of these approaches (especially glycemic control) on cognition were limited [5]. Therefore, there is an urgent need to clarify the neuropathological mechanism underlying diabetes-associated cognitive dysfunction and identify effective treatment approaches.

The hippocampus, which plays a pivotal role in maintaining cognitive function, is the main brain region affected in patients with diabetes [6]. The function of the hippocampus depends on communication among neurons, and synapses are the basic information-processing units that mediate communication between neurons. Synaptic damage and loss are central to hippocampal dysfunction, leading to impaired hippocampus-dependent cognitive function [7–9]. Several studies have suggested that hippocampal synaptic loss was the early critical pathological feature of diabetes-associated cognitive dysfunction and was strongly correlated with cognitive decline [6, 10, 11]. The cause of hippocampal synaptic loss in diabetes has yet to be fully elucidated, and further exploration is needed to determine the underlying mechanism.

Synapses are constantly formed and eliminated to maintain a delicate balance, and synaptic loss occurs when this balance is disrupted [12]. Hormones are powerful modulators of synapse formation and elimination. The modulatory actions of peripheral hormones on synapses have been reported to be involved in the regulation of cognitive function in diabetes. For example, in diabetes, insulin [13, 14], leptin [15] and incretins [16, 17] have neuroprotective effects by promoting synapse formation, whereas glucocorticoids induce neuropsychiatric impairments by exacerbating synaptic elimination [18, 19]. On the other hand, the role of central nervous system-derived hormones in cognitive dysfunction in diabetes has raised concerns, as melatonin has been reported to upregulate synapse-related proteins and alleviate cognitive impairment in diabetes [20]. The pituitary is the master endocrine gland of the central nervous system [21] and hormones secreted by the pituitary gland have various effects on hippocampal synapse regulation [22–25]. It remains unclear whether pituitary hormones are related to diabetes-associated cognitive dysfunction.

This study aimed to investigate the relationship between pituitary hormones and diabetes-associated cognitive dysfunction. Based on the results of our clinical research, we speculated that the pituitary hormone prolactin (PRL) was involved in the development of cognitive dysfunction in diabetes. Subsequent animal studies confirmed the deleterious effects of PRL deficiency on cognitive function in diabetes and revealed the cell-specific mechanism involved. Moreover, we found that PRL infusion therapy improved cognitive impairment in diabetic mice, providing an attractive therapeutic target for promoting cognitive health in diabetes.

Methods

Clinical cohort study

Participants. This study was conducted from January 2017 to October 2022 at Nanjing Drum Tower Hospital, The Affiliated Hospital of Nanjing University Medical School. All participants were right-handed and possessed > 6 years of education. T2DM diagnosis was based on the American Diabetes Association criteria [26] and menopause was diagnosed as 12 months of amenorrhea without a pathological cause. Exclusion criteria were: (1) hyperprolactinemia or pregnancy or parturition, (2) hormone or steroid treatment or drugs that modulate ovarian steroid secretion in 6 months prior to the study, or oral contraceptive use in 6 months prior to the study, (3) premenopausal and perimenopausal women, (4) history of neurological and psychiatric disorders, (5) dysfunction of organs including heart, liver or kidney, (6) thyroid diseases, (7) Acute complications such as diabetic ketoacidosis, hyperglycemic hyperosmolar state, or hypoglycemic coma within 6 months. Written informed consent was obtained from all participants.

Clinical measurements

Resting blood pressure, height, weight of patients were collected. Plasma glucose, insulin, and C-peptide concentrations were detected at fasting. Serum fasting total cholesterol (TC), triglyceride (TG), high density lipoprotein cholesterol (HDL-C), low density lipoprotein cholesterol (LDL-C), and glycated hemoglobin A1c (HbA_{1c}) concentrations were measured. Insulin resistance was estimated by the HOMA2 Calculator (HOMA2 v2.2.3; Diabetes Trials Unit, University of Oxford). Serum pituitary hormones included prolactin (PRL), follicle stimulating hormone (FSH), luteinizing hormone (LH), thyroid stimulating hormone (TSH), adrenocorticotropic hormone (ACTH) and growth hormone (GH) were measured by an automated chemiluminescent immunoassay (Siemens Immulite 2000, Germany) at 8:00 a.m. All patients fasted for 10 h and stayed quietly for 10 min before the measurement of serum pituitary hormones.

Cognitive assessments

General cognition was evaluated by Mini-Mental State Examination (MMSE) [27] and Montreal cognitive assessment (MoCA, Beijing Version) [28]. MCI was diagnosed according to the established criteria [29]: (1) Cognitive concerns from patients, informants or skilled clinicians. (2) Objective evidence of impairment in cognitive domains, which was demonstrated as subjects whose education-adjusted MoCA scores were less than 26. (3) Preservation of independence in functional abilities. Independence in daily functioning was evaluated by Activities of Daily Living. (4) Lack of evidence for dementia. Multiple cognitive subdomains, including immediate memory, visuospatial constructional, language, attention, and delay memory, were evaluated by the Repeatable Battery for the Assessment of Neuropsychological Status (RBANS) [30]. Processing speed was evaluated by the Trail Making Test (parts A and B) [31], and executive function was assessed by the completion time of Stroop Color-Word Test (parts I, II, and III) [32].

MRI data acquisition and analysis

Image data were obtained using a 3.0T MR scanner (Achieva TX; Philips Medical Systems, Eindhoven, Netherlands) with an 8-channel head coil. Structural data were acquired with high-resolution T1-weighted three-dimensional fast field echo structural scans (repetition time 9.7 ms, echo time 4.6 ms, field of view 256 mm×256 mm×192 mm, flip angle 8°, and voxel size 1 mm×1 mm×1 mm). Segmentation of hippocampal subregions was accomplished by FreeSurfer software 7.2 (Athinoula A. Martinos Center for Biomedical Imaging, USA). A 3D image of the right hippocampus was established using 3D Slicer software 5.2.1 (National Inst. Of Health, USA).

Animal studies

The PRL knockout (PRL KO) mice were generated by using CRISPR/Cas 9 technology to modify the PRL gene. The brief process was as follows: sgRNA was transcribed in vitro, Cas9 and sgRNA were microinjected into fertilized eggs of C57BL/6 mice to obtain F0 generation mice. The correct F0 generation positive mice were mated with C57BL/6 mice to obtain a stably heritable F1 generation positive mouse model as verified by PCR-sequencing. The offspring were genotyped by PCR with the following primers: wild type (WT) alleles: GPS00003371-Prl-KO-tF1 5′-AACAGTATGTGCAAGACCGTG-3′ and-GPS00003371-Prl-KO-tR1 5′-TGGACAGTTTATGGC TCAGCTAC-3′; PRL KO alleles: GPS00003371-Prl-KO-tF1 5′-CAGCTAGTGAGCTATTTAACAGTGCTG-3′ and GPS00003371-Prl-KO-tR1 5′-TCAGCCAAACTCA TGGATAGAGG-3′.The sequence of sgRNA and experiments to verify that PRL is not expressed are presented in Supplementary Fig. S5. Cx3cr1CreERT2 mice were crossed with PRLRfl/fl mice (purchased from the Model Animal Research Center of Nanjing University). Microglial PRLR conditional knockout (cKO) mice were generated after we treated Cx3cr1CreERT2: PRLRfl/fl mice with tamoxifen (TAM) at different stages indicated. After TAM induction, mice were randomly divided into two groups and fed either a normal chow diet (5010, LabDiet, USA) or an HFD diet (D12492, Research Diets, USA) for 12 weeks. All mice were housed in a specific-pathogen-free facility under a 12-h light-dark cycle with food and water available ad libitum.

PLX3397 and minocycline treatment

A total of 38 mice were treated with PLX3397 or its vehicle. PLX3397 was dissolved in 5% DMSO (HY-Y0320, MCE, USA) and 40% PEG300 (HY-Y0873, MCE, USA) in ddH_2O. WT and PRL KO mice were treated with PLX3397 (1029044-16-3, MCE, USA) by oral gavage using a gavage needle. Treatment with PLX3397 was administered at a dose of 50 mg/kg per day for 4 weeks. A total of 39 mice were treated with minocycline or saline. Minocycline was purchased from Sigma Aldrich (M9511, Canada). WT and PRL KO mice were intraperitoneally injected with minocycline or saline for one month at a dose of 50 mg/kg/day.

Tamoxifen injection

Tamoxifen injections were performed in 35 $Cx3cr1^{CreERT2}$: $PRLR^{fl/fl}$ mice and 34 $PRLR^{fl/fl}$ mice. Tamoxifen (HY-13757A, MCE, USA) was dissolved in 10% ethanol and 90% corn oil. Mice were injected with tamoxifen intraperitoneally once every 24 h for one week, with a dose of 75 mg tamoxifen/kg body weight (20 μg/μl).

Viral injection

A total of 20 C57BL/6 mice accepted the virus injection. Adeno-associated virus (AAV) adenoviruses expressing short-hairpin RNA (shRNA) specific for neuronal PRLR or scrambled shRNA were obtained from brain-VTA (Wuhan, China). AAV-hSyn-EGFP-shRNA (PRLR) or scramble were infused into the bilateral hippocampus (anteroposterior=-2.8 mm, mediolateral=±3.0 mm, dorsoventral=-2.85 mm). The shRNA sequence for mouse PRLR was 5′-GCCACCTACCATAACTGATGT-3′. The virus (titer: 5e+12vg/ml) was infused at a rate of 200nl/min (1.0 μl/side) followed by a 10-min of rest.

Intracerebroventricular injection of PRL

A total of 20 chow diet-fed mice and 20 high fat diet-fed mice accepted the intracerebroventricular injection of PRL or its vehicle. Osmotic pumps (1001 W, RWD, China) were loaded with recombinant murine PRL (321-10, PrimeGene, China) supplemented with 0.1% BSA or vehicle solution (PBS, containing 0.1% BSA), attached to the infusion cannula. The cannula was implanted in right lateral ventricle (anteroposterior=+0.3 mm, mediolateral=+1.0 mm, dorsoventral=-2.5 mm) and fixed to the skull for intracerebroventricular infusion. Mice implanted with pumps received 0.8 μg of PRL per day over a 4-weekes period at a flow rate of 0.25 μl/h.

Behavioral analysis

Open field (OF)

The open filed test was performed as previously described [33]. Test was performed in a 48 cm×48 cm×36 cm open field box. Mice were placed in the center of the open field box and allowed to explore freely. The box was cleaned with 75% ethanol between the trials. We quantified the total distance the mice traveled within 5 min and the mean speed with ANY-maze software 7.0 (Stoelting Co., IL, USA).

Novel object recognition test (NORT)

The NORT was carried out as the method described previously [34]. The test was conducted in a grey open field box (48 cm width×48 cm depth×36 cm height). Mice were positioned in the open field box with two identical objects and allowed to behave freely for 10 min. Replacing one of the old objects with a new object with the same size but a different shape. Each mouse was allowed to explore the open field for 5 min. The time mice spent on exploring the novel and the familiar objects was recorded by a video tracking system. The box was cleaned with 75% ethanol after testing of each animal to diminish olfactory cues. The discrimination index was calculated as ([novel object exploration time/total object exploration time] ×100%).

Morris water maze (MWM)

Learning and memory performance was assessed by MWM according to the previously described method [35]. A 120-cm circular pool was divided into four equal quadrants (northeast, southeast, southwest, and northwest). The procedures consisted of 1 day of the visible platform test, four 60s trials per day for 5 consecutive days of the hidden platform test and a probe trial. During 5 days of hidden platform training, the platform was placed in the middle of the northeast quadrant at 1 cm underneath the water surface. The starting points for releasing mice into water were equally distributed among the four maze quadrants. Time taken by the mouse to find and climb onto the platform was recorded as latency. If the mice were unable to find the hidden platform within 60s, the mice were guided onto the platform manually and allowed a rest on the platform for 15s. In the probe trial, each mouse was placed into the water in the opposite quadrant, and the percentage of total time in target quadrant was measured. Tracking of animal movement was recorded with a DigBehv-MM tracker system (MobileDatum Co. Ltd, China).

Glucose tolerance test and insulin tolerance test

For glucose tolerance tests, basal blood glucose levels of mice were measured, followed by intraperitoneal injection with 2g/kg weight glucose after a 12-h fast. Blood glucose levels were recorded after 15, 30, 60 and 120 min using blood obtained via the tail vein. For insulin tolerance tests, basal blood glucose levels of mice were measured, followed by intraperitoneal injection with insulin (0.5 unit/kg body weight) after a 4-h fast. Blood glucose levels were recorded after 15, 30, 60 and 120 min using blood obtained via the tail vein.

Cell cultures and treatments

Primary microglial culture

Primary microglia were isolated from mixed glia harvested from newborn WT mice and PRL KO mice. After 12–14 days in culture, the microglia on the mixed primary glia layer were isolated by shaking the flasks. Cells were seeded into 24-well plates with DMEM/F12 complete medium plus 10% fetal bovine serum and 1% penicillin/streptomycin. Primary microglia were treated with recombinant PRL protein (321-10, PrimeGene, China) (100ng/ml) or minocycline (20μM) for 24 h before engulfment test.

Microglial engulfment test in vitro

Equal amounts of pHrodo-green conjugated synaptosomes were added to cultured WT or PRL KO microglia. After 1.5 h of incubation with synaptosomes, microglia were washed in PBS and fixed in 4% paraformaldehyde (PFA) for 10 min. After fixation, microglia were washed

again in PBS and blocked with 5% bovine serum albumin (BSA) with 0.3% triton-X 100 in PBS for 1 h at room temperature. Microglia were then incubated with primary antibody overnight at 4 °C, followed by secondary fluorescent antibody staining for 1 h at room temperature. Microglia were stained with DAPI for 10 min and rinsed twice with PBS before imaging with a Leica TCS SP8-MaiTai MP confocal microscope (Leica, Germany). The whole experiment was performed in the dark.

Adult microglia isolation

Mice were anaesthetized and perfused intracardially with ice-cold Dulbecco's phosphate-buffered saline to obtain brains. The Adult Brain Dissociation Kit (130-107-677, Miltenyi Biotec, Germany) was used to prepare a single-cell suspension after tissue dissociation, debris removal and erythrocyte removal. Microglia were further isolated from the single cell suspension using MACS Separation Columns (MS) (130-042-201, Miltenyi Biotec, Germany) and magnetic CD11b microbeads (130-093-634, Miltenyi Biotec, Germany). The isolated microglia were treated with or without a Rap1 inhibitor (GGTI298, MCE, USA) before engulfment test.

RNA sequencing and analysis

Total RNA was extracted from microglia followed by library preparation according to Illumina standard instruction (VAHTS Universal V6 RNA-seq Library Prep Kit for Illumina®, Vazyme, China). Agilent 4200 bioanalyzer was employed to evaluate the concentration and size distribution of cDNA library before sequencing with an novaseq6000 (Illumina, USA). The protocol of high-throughput sequencing was fully according to the manufacturer's instructions (Illumina). The raw reads were filtered by Seqtk before mapping to genome using Hisat2 (version:2.0.4). The fragments of genes were counted using stringtie (v1.3.3b) followed by TMM (trimmed mean of M values) normalization. Standard DESeq2 v1.42.0 workflow was then applied to the count matrix to identify DEGs. *P*-values were obtained with the Wald test and corrected by the BH method. Differentially expressed genes (DEGs) were defined by adjusted p-value < 0.05 and $|\log_2 \text{FoldChange}| > 0.26$ (equivalent to 1.2-fold change).

Quantitative real-time PCR

In brief, total RNA was isolated by TRIzol reagent (15596018, Invitrogen, USA), and then cDNAs were synthesized using the Evo M-MLV PT Premix for PCR (AG11706, AG, China). cDNAs were amplified by quantitative real-time RT–PCR using a SYBR Green kit (AG11701, AG, China). Data were collected by a real-time PCR machine (Roche LightCycler 480II, Switzerland) and its software. Levels of gene expression were normalized relative to glyceraldehyde-3-phosphate dehydrogenase (GAPDH). The primer sequences of genes were taken from literature [36] or Primer Bank. Primer sequences were listed in Table S1.

Western blotting

Mouse hippocampus tissues were washed with ice-cold PBS and lysed in lysis solution including RIPA buffer (89900, Thermo, USA) and phenylmethyl-sulphonyl fluoride (PI0011, LEAG ENE, China) on ice for 0.5 h, and centrifuged for 0.5 h at 13,000 rpm. The supernatants were transferred into new 1.5 ml-tubes and boiled in SDS loading buffer. After SDS–PAGE, proteins were separated on 10% SDS-polyacrylamide gels and transferred to polyvinylidene difluoride (PVDF) membranes. The membranes were incubated with the following primary antibodies at 4 °C overnight: rabbit anti-Prolactin (1:1000, Abcam, ab188229), rabbit anti-Prolactin receptor (1:1000, Abcam, ab170935) and rabbit anti-β-actin (1:1000, Bioworld, AP0060). After washing with 0.1% Tris-buffered saline with Tween (TBST), the membranes were incubated with secondary antibodies (1:5000, Biosharp, BL023A) at room temperature for 1 h. The color detection was carried out with an ECL Western Blotting Detection kit (180-5001, Tanon, China), and quantified by Fiji-ImageJ software 1.0 (National Inst. Of Health, USA).

Enzyme-linked Immunosorbent Assay (ELISA)

To determine the concentrations of PRL in mouse serum, ELISA assay was performed according to the manufacturer's instructions by using Mouse Prolactin ELISA Kit (FMS-ELM117, FMS, China). To detect the production of inflammatory factors in hippocampus, ELISA assays were performed by commercially available ELISA kits (BioLegend, China).

Immunofluorescence and image analysis

Briefly, mouse brains were fixed in 4% PFA for 24 h, then soaked in 15% and 30% sucrose solution for dehydration. We use a Leica cryostat (Leica CM1950) to cut coronal sections of 25 μm. Brain sections were incubated in 5% BSA with 0.3% triton-X 100 in PBS for 1 h at room temperature. Then sections were incubated with primary antibodies at 4 °C overnight. After washing with PBS for three times, the sections were incubated with secondary antibodies for 1 h at room temperature. Tissue sections were stained with DAPI and rinsed three times with PBS before image capture. For primary cultured cell immunofluorescence, cells were fixed with 4% PFA for 10 min, and the following procedure was the same as brain tissues. Information of antibodies used were summarized in Table S2.

Synaptic density in vivo

In brief, 25 μm sections stained with synaptic markers (Vglut1/NeuN, Vglut1/PSD95) were captured by Leica TCS SP8-MaiTai MP confocal microscope (Leica, Germany). Captured images were used to quantify the number of colocalized pre- and post-synaptic puncta. Single-channel images were used to quantify single synaptic marker density by Fiji-ImageJ software 1.0 (National Inst. Of Health, USA). Synaptic density was determined as puncta given area (276 μm×276 μm).

Fluorescent intensity

Images were converted into 8-bit to obtain total gray value in given area (562 μm×562 μm) by Fiji-ImageJ software 1.0 (National Inst. Of Health, USA). The fluorescent intensity was calculated as follows: gray value (CD68)/(Iba-1).

Cell number

For hippocampal neuron counting, the number of neurons was quantified by $NeuN^+$ cell number in a square field (750 μm×750 μm). Immunofluorescence–stained images of $NeuN^+$ cells were captured by a Leica TCS SP8-MaiTai MP microscope (Leica, Germany). Images were converted to 8-bit, and cells were cropped and thresholded to produce a binary (black and white) image. The number of cells were manually counted by using the cell counter plugin for the Fiji-ImageJ software 1.0 (National Inst. Of Health, USA). Five brain sections per mouse were used for neuronal counting. The number of neurons in the experimental groups was normalized to the number of neurons in the control group (cell count in experimental group/cell count in control group*100%). For hippocampal microglia counting, the number of $Iba\text{-}1^+$ cells was divided by the total area (3072 μm×2048 μm) of the acquired field to represent cell density. The z-stack images of Iba-1 stained hippocampal slices were acquired by a Leica TCS SP8-MaiTai MP microscope (Leica, Germany). After being performed z-stack projection, the images were converted to 8-bit. Cells were cropped and thresholded to produce a binary (black and white) image, and then automatically counted using the particle analyzer plugin for the Fiji-ImageJ software 1.0 (National Inst. Of Health, USA). Three brain sections per mouse were used for microglial counting and microglia number displayed as cells per square millimeter. The threshold for NeuN and Iba-1 kept constant during image analyses.

3D microglial engulfment quantification

Z-stack images (at 0.3 μm intervals) were captured by Leica TCS SP8-MaiTai MP confocal microscope (Leica, Germany). Images were captured by choosing microglia with Iba-1 positive channel randomly. Images were processed by subtracting background using ImageJ software. Afterwards, 3D volume surface renderings of each z-stack were created using Imaris 9.0 software (Bitplane, Switzerland). Surface rendered images were used to calculate the volume of the microglia and synaptic puncta. Engulfment percentage was calculated as volume of internalized synaptic volume of microglia.

2D microglial engulfment assay in vitro

Engulfment was analyzed by calculating the fraction of the Iba-1 area overlapped by the pHrodo area. Cells were imaged using Leica TCS SP8-MaiTai MP confocal microscope (Leica, Germany).

Synaptosome isolation and pHrodo labeling

Mouse forebrains were quickly removed and homogenized in ice-cold gradient buffer (320.0 mM sucrose, 5.0 mM HEPES, 0.1 mM EDTA, pH 7.5) (HEPES, 2185833, Thermo scientific, USA; EDTA, AM9260G, Thermo scientific, USA). The homogenate was centrifuged at 1000×g for 20 min to collect supernatant, and supernatant was centrifuged at 1200×g for 10 min. The supernatant was centrifuged at 10,000×g for 10 min to obtain pellet. The pellet was resuspended in gradient buffer and loaded onto a sucrose gradient (0.8 M:1.2 M = 1:1). The layer between 0.8 M sucrose and 1.2 M sucrose was collected carefully after centrifugation at 100,000×g for 1 h. Equal volume of ultrapure water was added to dilute the collected layer before centrifuged at 100,000×g again to acquire the purified synaptosome pellet. For pHrodo labeling, synaptosomes were incubated with pHrodo Green STP ester (P36013, Thermo scientific, USA) in sodium carbonate buffer pH 9.0 for 2 h at 4 °C in the dark. After incubation unconjugated pHrodo was washed by PBS.

Statistical analysis

SPSS software 26.0 (IBM, IL, USA) and GraphPad Prism software9.0 (GraphPad, USA) were used for statistical analysis. Data were analyzed using unpaired two-tailed *t* test, Mann-Whitney *U* test, one-way ANOVA analysis and post hoc tests (Dunnett's multiple comparisons test), two-way ANOVA analysis (followed by Sidak's multiple comparisons test) and Kruskal-Wallis analysis. Normality of data was tested by Shapiro-Wilk test (for a sample size < 50) or Kolmogorov-Smirnov test (for a sample size ≥ 50). Heterogeneity of data was tested by F-test. Relative weight (RW) analysis was performed as the reported method [37]. All tests used for statistical analyses were mentioned in the figure legends. *P* values of 0.05 or less were supposed to be statistically significant.

Results

Lower serum PRL levels were associated with cognitive impairment and decreased hippocampal volume in T2DM patients

A total of 744 T2DM patients including 445 men and 299 postmenopausal women were enrolled. The flowchart of sample selection is presented in Supplementary Fig.S1. Subjects were 58.9±7.2 years and the average years of education was 12.3±3.7 years. Mean duration of diabetes were 10.5±8.0 years. According to the diagnostic criteria for MCI, subjects were divided into T2DM cognitively normal group (476 individuals) and T2DM with MCI group (268 individuals). The T2DM with MCI group possessed less education and had a higher proportion of female and smokers, and exhibited unfavorable metabolic profiles (e.g. higher levels of SBP, HbA_{1c}, FBG, FINS, HOMA-IR, but lower levels of FCP, all $P<0.05$). Regarding pituitary hormones, T2DM patients with MCI had lower serum PRL levels and higher FSH and LH levels compared to cognitively normal T2DM patients (Table S3 and Fig.S2). Logistic regression model indicated that only lower serum PRL level was associated with a higher risk of MCI (odds ratio (OR): 0.731 [95%*CI* 0.664–0.805], $P<0.001$) after adjustment for age, sex, education, SBP and glycemic-related characteristics (Fig. 1A). Furthermore, relative weight analysis revealed that serum PRL level carried a relative weight of 82.76% in the MCI risk prediction model (Fig. 1B), contributing much more than other pituitary hormones (FSH, 7.16%; LH, 5.01%; TSH, 1.35%; ACTH, 3.69%; GH, 0.04%). These observations suggested that the low PRL level, but not other pituitary hormones, was an important independent predictor of MCI in T2DM patients. Similarly, gender subgroup analysis demonstrated that serum PRL levels were diminished in MCI patients compared to controls in both men and women, and low PRL levels were linked to an increased risk of MCI in both genders (men OR: 0.873 [95%*CI* 0.786–0.969], $P=0.010$; women OR: 0.584 [95%*CI* 0.488–0.699], $P<0.001$) (Table S4-5 and Fig.S3).

To further identify the relationship between serum PRL levels and cognitive impairment in T2DM, patients were divided into four groups according to serum PRL quartiles (Table S5). The quartile ranges of Q1, Q2, Q3, and Q4 of serum PRL levels were <4.88, 4.88–6.27, 6.27–7.84, and ≥7.84 μg/L. With decreasing PRL quartiles, the prevalence of MCI increased (Q4, 17.1%; Q3, 40.5%; Q2, 41.7%; Q1, 55.8%, $P<0.001$) (Fig. 1C). Taking Q4 as the reference group, the risk of MCI gradually increased in the three lower quartiles (Adjusted OR_{Q3VSQ4}: 4.723 [95% *CI* 2.683–8.315]; OR_{Q2VSQ4}: 4.793 [95% *CI* 2.687–8.548]; OR_{Q1VSQ4}: 6.411 [95% *CI* 3.552–11.574], all $P<0.05$) (Fig. 1D).

Next, we found that the deleterious effects of low PRL level on cognitive function might concern several domains. Correlation analysis indicated that serum PRL levels were positively associated with immediate memory ($r=0.231$, $P<0.001$), visuospatial construction ($r=0.196$, $P<0.001$), attention ($r=0.183$, $P<0.001$) and delayed memory ($r=0.139$, $P=0.001$), while serum PRL levels were negatively linked to processing speed (time) (r = -0.189, $P<0.001$). These correlations relationships persisted after adjustment for age, education and sex (Fig. 1E).

Magnetic resonance imaging (MRI) techniques offer a noninvasive approach to detect subtle brain alterations before clinical symptoms of cognitive impairment occur. To investigate the underlying changes in brain structure, subjects in four quartiles who had no MRI complications underwent MRI scans (Q1, $n=52$; Q2, $n=48$; Q3, $n=42$; Q4, $n=70$). No significant differences existed in demographics, clinical characteristics, cognitive function and pituitary hormone levels between the total sample and the MRI subsample (Table S6). The volumes of total intracranial, gray matter and white matter were similar among the four quartiles (Table S7). Subjects in Q1 showed significantly reduced volume of hippocampus compared to subjects in Q4 (2756.49±369.20 vs. 2967.90±375.57mm^3, $P=0.001$) after controlling for age, sex, education and total intracranial volume (TIV) (Fig. 1F). The hippocampal subregions and surrounding regions were labeled (Fig. 1G). Subjects in Q1 showed decreased volumes in subfields of bilateral CA1, CA3, CA4, GC-DG and subiculum comparable to those in Q4 (Fig. 1H). The collective results suggested that hippocampal damage might involve in the adverse effects of the decreased PRL level on cognitive performance.

Decreased PRL levels precede cognitive deficits and hippocampal synaptic loss in HFD-diabetic mice

To further investigate whether the changes of PRL levels involved in diabetes-associated cognitive dysfunction. mice were dynamically fed with a chow diet (CD) or a HFD (kcal%: fat, 60%; carbohydrate, 20%; protein, 20%). Evaluation of PRL levels, behavioral tests and immunofluorescent staining were conducted at three consecutive time points with an interval of 4 week (week 4, 8, and 12) (Fig. 2A). When dynamically compared with CD mice, HFD mice displayed reduced serum PRL levels and hippocampal PRL protein levels since week 8 (Fig. 2B-C). The cognitive deficits of HFD mice occurred at week 12, presenting with reduced novel object preference, increased time to reach the invisible platform, reduced preference for target quarter, and decreased number of platform entries (Fig. 2D-G). Notably, we observed hippocampal synaptic loss in HFD mice at week 12 (Fig. 2H-I, K-L), whereas no significant difference existed in the density of neuronal marker NeuN at all three time points between two fed groups (Fig. 2H, J), suggesting that the

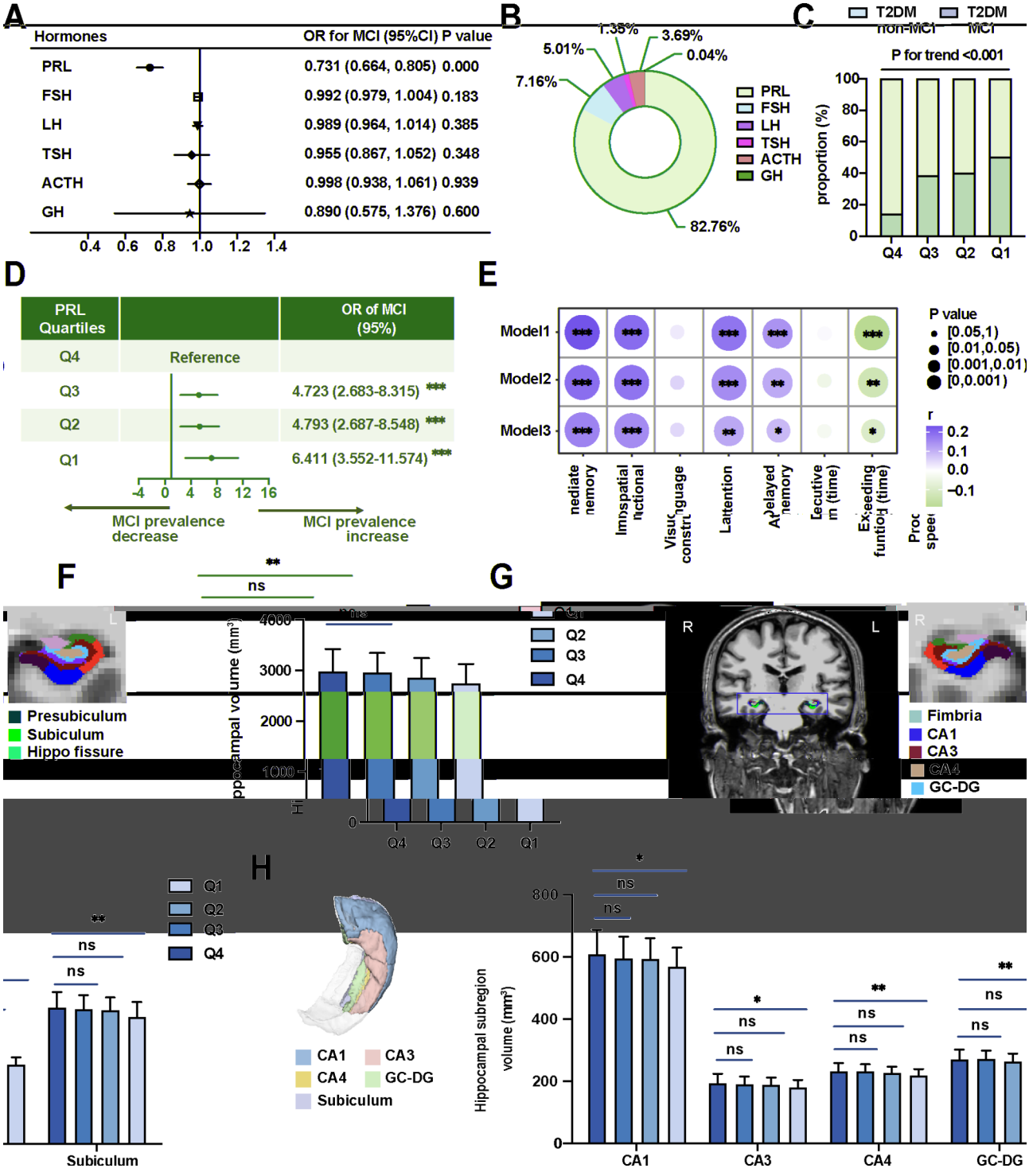

Fig. 1 Serum PRL levels were associated with MCI and decreased hippocampal volumes in T2DM patients. (**A**) Associations between levels of pituitary hormones and risk of MCI were adjusted for age, education, sex, smoking, SBP, FBG, FINS, FCP, HbA_{1c}, HOMA-IR. (**B**) Relative weight analysis of pituitary hormones in MCI prediction model. (**C**) Associations between quartiles of serum PRL levels and the prevalence of MCI. (**D**) Odds ratio (OR) of MCI according to quartiles of serum PRL levels were adjusted for age, education, sex, SBP, DBP, TC, HDL-C, LDL-C, FBG, HOMA-IR. Q4 is the reference group. (**E**) Associations between serum PRL levels and multiple cognitive subdomains. Model 1 was unadjusted. Model 2 was adjusted for age. Model 3 was adjusted for age, education and sex. (**F**) Associations between quartiles of serum PRL levels and the volumes of hippocampus after controlling for age, education, sex and TIV. (**G**) An example of Freesurfer v.7.2 hippocampal segmentation with coronal. (**H**) Comparisons about the volumes of hippocampal subregions (CA1, CA3, CA4, GC-DG and subiculum) between quartiles of serum PRL levels. Data are presented as the mean ± SD. *$p < 0.05$, **$p < 0.01$, and ***$p < 0.001$; ns, not significant; one-way ANOVA (**F**, **H**)

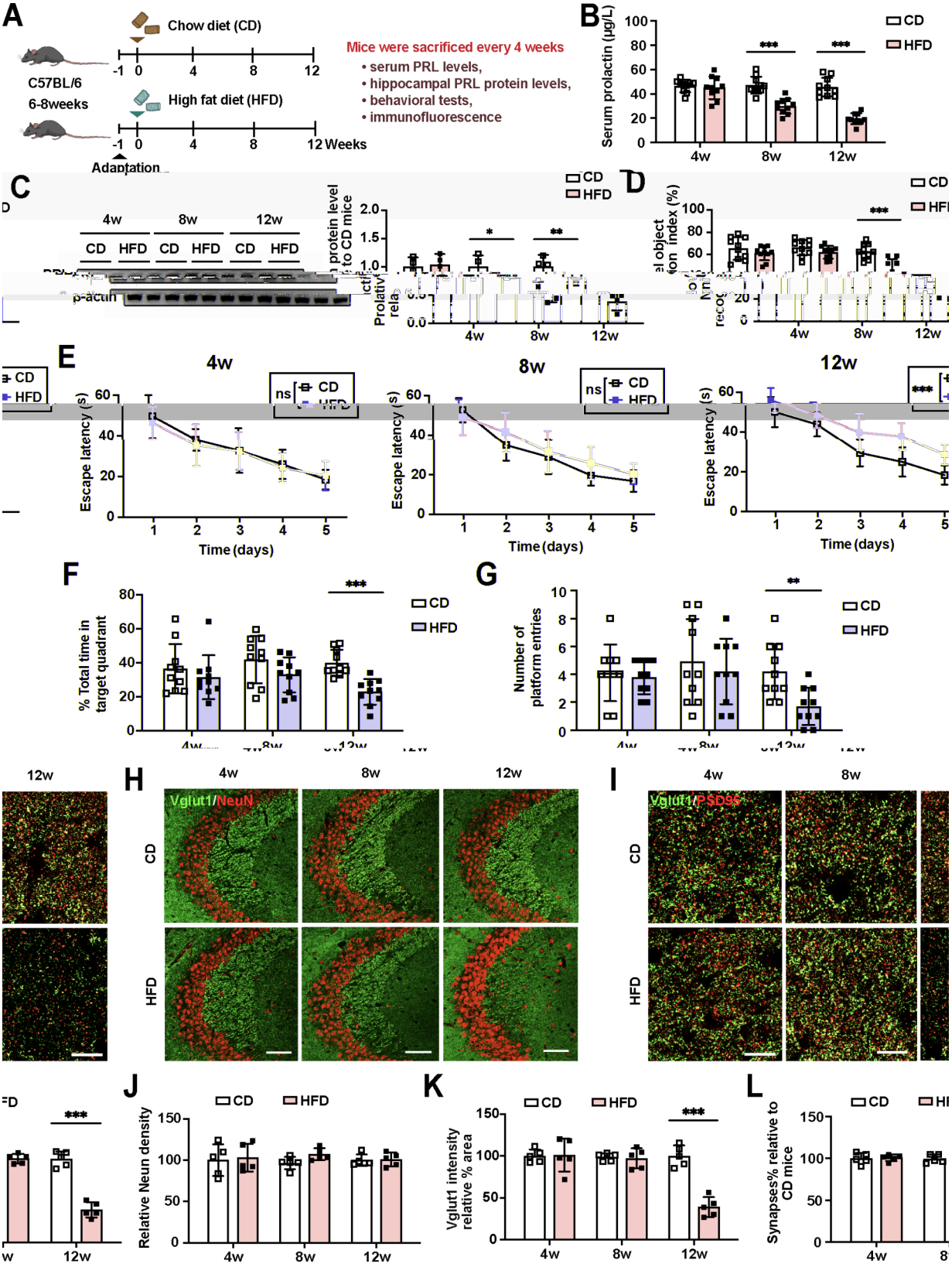

Fig. 2 (See legend on next page.)

(See figure on previous page.)

Fig. 2 Decreased PRL level predated cognitive impairment and synaptic loss in HFD-diabetic mice. (**A**) Experimental design. (**B**) Serum PRL levels in chow diet mice and high food diet mice. (**C**) PRL protein levels in hippocampus of chow diet mice and high food diet mice. (**D-G**) Behavioral tests of mice fed by chow diet or high fat diet for 4, 8 and 12 weeks. Novel object recognition index (**D**), escape latencies (**E**), % total time in the target quadrant (**F**), number of platform entries in probe trial (**G**). (**H**) Representative confocal images of NeuN (red) and Vglut1 (green) in CA3 region of hippocampus. Scale bar, 80 μm. (**I**) Representative confocal images depict synaptic staining for pre-synaptic marker Vglut1 (green) and post-synaptic marker PSD95 (red) in CA1 region of hippocampus. Scale bar, 15 μm. (**J**) Relative number of neurons. (**K**) Relative level of Vglut1 intensity. (**L**) Relative level of hippocampal pre- and post-synaptic density. Data are presented as the mean ± SD. $n = 10$ mice/group (**B**, **D-G**) and $n = 4$-5 mice/group (**C**, **J-L**). *$p < 0.05$, **$p < 0.01$, and ***$p < 0.001$; ns, not significant; two-way ANOVA (**E**) or unpaired two-tailed *t* test (**B-C**, **F-L**)

hippocampal synaptic loss, not neuronal loss, might underlie impaired cognitive function in the early stages of diabetes. Altogether, these data demonstrated that in HFD-diabetic mice, decreased PRL levels preceded cognitive impairment and hippocampal synaptic loss, suggesting that decreased PRL levels might contribute to the development of diabetes-associated cognitive dysfunction.

PRL KO mice exhibited cognitive impairment and hippocampal synaptic loss

To determine whether the deficiency of PRL directly act on cognitive function and hippocampal synapse density, we generated PRL KO mice (Fig. 3A and Fig. S5A-B) by using CRISPR/Cas 9 technology. Mice were fed a chow diet and had similar body weights (Fig. S5C). The performance of mice in the new object recognition test and the Morris water maze task was tested. Compared with wild-type (WT) mice, PRL KO mice had longer escape latencies in the hidden platform test, smaller number of platform entries in the probe trial, and spent less time in the target quadrant in the probe trial and object recognition test. (Fig. 3B-E). These results indicated that knockout of PRL significantly impaired learning and memory. Furthermore, immunostaining revealed a reduction in the pre-synaptic marker Vglut1 and the post-synaptic marker PSD95 in the hippocampus of PRL KO mice, without any alteration in neuronal numbers (Fig. 2F-J). These results suggested that knockout of PRL led to hippocampal synaptic loss, and neuronal loss might not be the reason for synaptic loss. Together, these data demonstrated that deficiency of PRL had deleterious effects on cognitive function and hippocampal synaptic density in mice.

The deleterious effects of PRL deficiency on cognitive function and hippocampal synaptic density were mediated by microglia

We proceeded to inquire as to which cell type is implicated in the effects of PRL deficiency on the development of cognitive dysfunction. PRL mediates its physiologic functions through the engagement of prolactin receptor (PRLR) [38]. We observed that PRLR was widely expressed in neuron and microglia but had little expression in astrocyte in hippocampus (Fig. 4A and Fig. S6E). To investigate whether microglia involved in the impacts of PRL deficiency on behavioral performance and hippocampal synapses, we took advantage of PLX3397. PLX3397 is a drug that decreases the microglial population without causing cognitive impairment in WT mice [39], and has been shown to reduce the secretion of PRL in mother mice [40]. After four weeks of PLX3397 treatment, there was a notable reduction in microglial numbers in hippocampus of WT and PRL KO mice, with no discernible alterations in PRL secretion in either mouse strain (Fig. 4B-D). Remarkably, depletion of activated microglia by PLX3397 in PRL KO mice fully rescued their cognitive deficits in novel objection recognition test and Morris water maze test (Fig. 4E-H). Furthermore, microglial depletion ameliorated hippocampal synaptic loss in PRL KO mice (Fig. 4I-M). These data suggested a mediate role of microglia for cognitive performance and synaptic damage caused by PRL deficiency. To further confirm this, we used a tamoxifen induced microglial PRLR conditional knockout mice (cKO) (Fig. S6F). Microglial PRLR cKO was confirmed by the fact that the microglial PRLR expression level was significantly eliminated in the hippocampus (Fig. S6G-I). Compared with control mice, microglial PRLR conditional knockout mice showed cognitive impairment and synaptic loss (Fig. 4N-V). In addition, we inhibited PRLR in hippocampal neurons by injecting adeno-associated virus (AAV) expressing shRNA against neuronal PRLR in the hippocampus (Fig. S7A-D). The inhibition of hippocampal neuronal PRLR failed to influence the cognitive performance and hippocampal synapse density (Fig. S7E-Q). These results confirmed that microglia were the primary contributors to cognitive impairment and synaptic damage resulting from PRL deficiency.

PRL deficiency led to cognitive impairment and hippocampal synaptic loss by enhancing microglial phagocytic capacity of synapses

Proinflammatory microglia cause neuroinflammation which in turn contributes to synaptic loss [41]. To investigate whether microglia-associated neuroinflammation is the underlying cause of PRL deficiency-induced synaptic loss, we measured the levels of inflammation factors in hippocampus of WT and PRL KO mice. The expression and secretion levels of inflammation cytokines (TNF-α, TNF-β, IL-1β, IL-4, IL-6, IL-10) in the hippocampus were not changed between two groups (Fig. S8A-G).

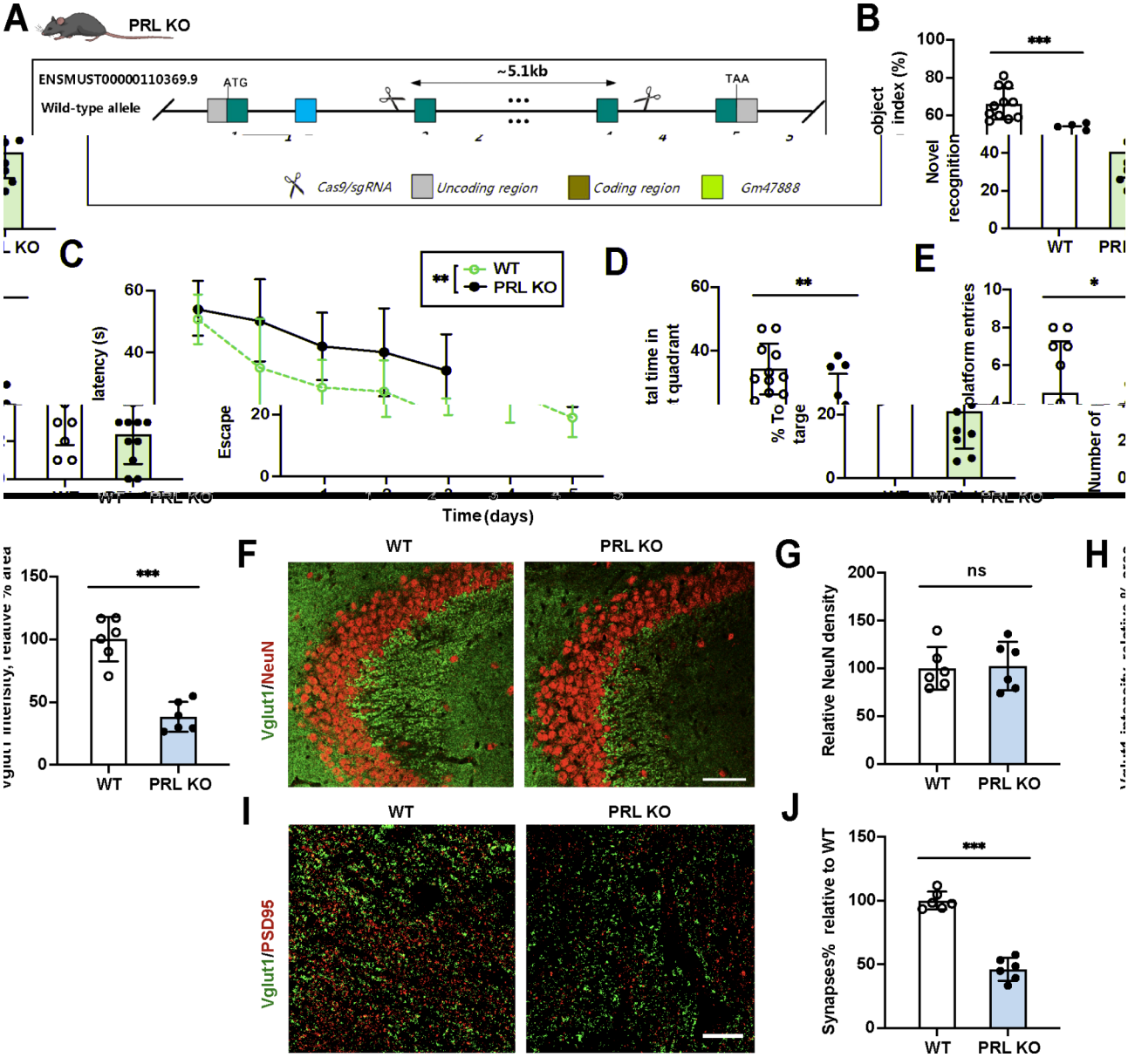

Fig. 3 PRL KO mice exhibited cognitive impairment and synaptic damage. (**A**) Experimental strategy used for generating PRL KO mice. (**B**) Quantitation of novel object recognition index in the novel objection recognition test. (**C**) Time spent in finding the hidden platform in Morris water maze (escape latency). (**D**) Percentage of time spent in the target quadrant in total time. (**E**) The number of platform entries in probe trial. (**F**) Representative confocal images of hippocampal immunostaining for neuronal marker NeuN (red) and pre-synaptic marker Vglut1 (green). Scale bar, 80 μm. (**G**) Relative NeuN density in hippocampus. (**H**) Relative level of Vglut1 intensity in hippocampus. (**I**) Representative confocal images depict synaptic staining for pre-synaptic marker Vglut1 (green) and post-synaptic marker PSD95 (red) in hippocampus of WT and PRL KO mice. Scale bar, 15 μm. (**J**) Relative level of hippocampal synaptic density. Data are presented as the mean ± SD. $n = 11$ mice/group (**B–E**) and $n = 6$ mice/group (**F–I**). *$p < 0.05$, **$p < 0.01$, and ***$p < 0.001$; ns, not significant; two-way ANOVA (**C**) or unpaired two-tailed *t* test (**B**, **D-J**)

These results indicated that the lack of PRL did not cause inflammation in hippocampus.

Abnormal phagocytosis of synapses by microglia is associated with synaptic loss [42, 43]. To explore whether the abnormal phagocytic ability of microglia is responsible for synapse density reduction, we checked the phagocytic activity of microglia in hippocampus. The protein levels of CD68 (a lysosome marker) were upregulated in hippocampus of PRL KO mice (Fig. 5A-B), suggesting that knockout of PRL increased the activity of microglial phagocytosis. We further used the 3D engulfment quantification method to analyze the number of synapses engulfed by microglia in hippocampus. There was a larger volume ratio of Vglut1$^+$ puncta in Iba-1$^+$ microglia in the hippocampus of PRL KO mice compared to WT mice, indicating that knockout of PRL enhanced phagocytic

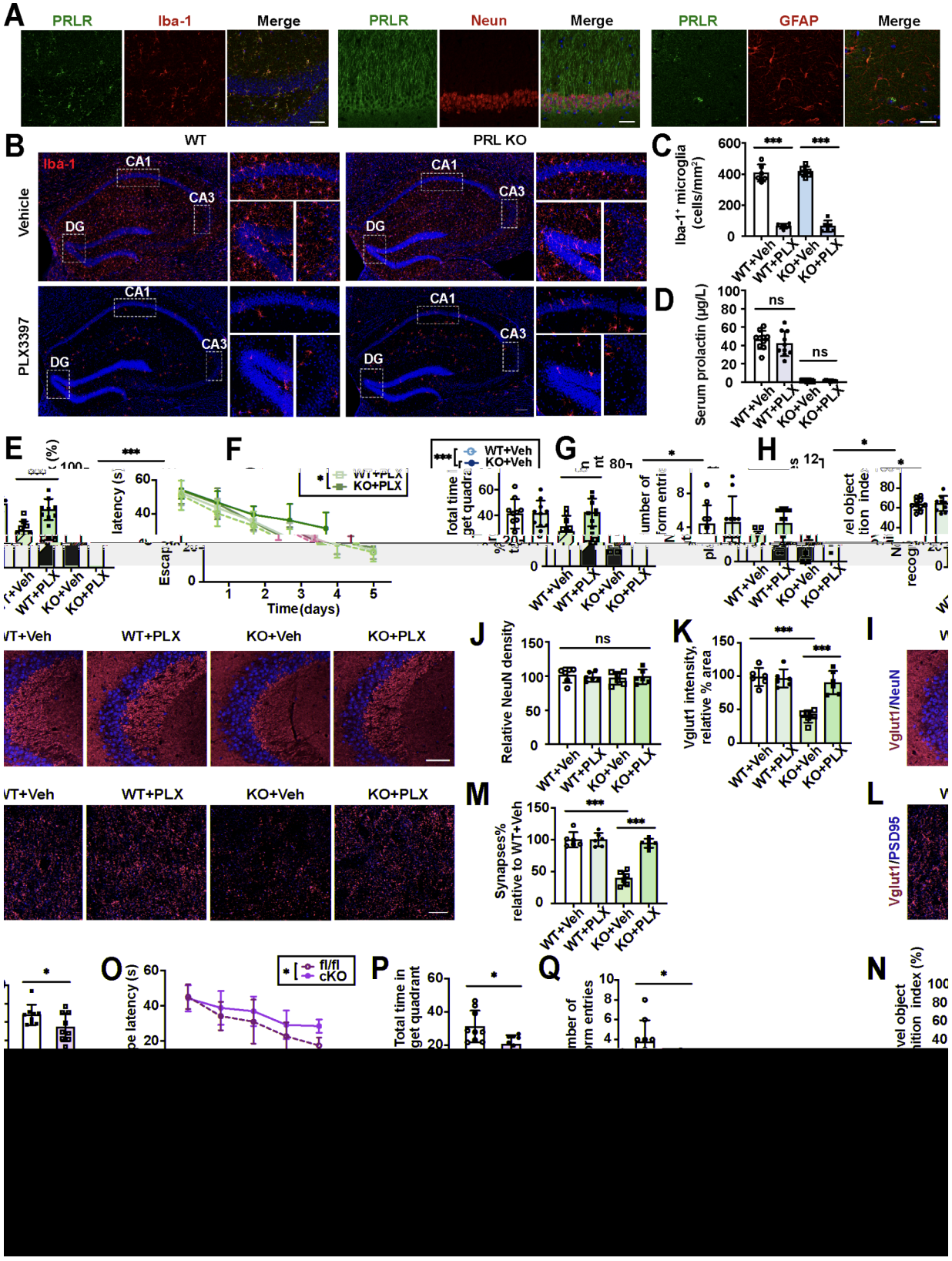

Fig. 4 (See legend on next page.)

(See figure on previous page.)

Fig. 4 The harmful effects of PRL deficiency on cognitive function and hippocampal synaptic density were mediated by microglia. (**A**) Immunostaining of PRLR with microglial marker (Iba-1), neuronal marker (NeuN) and astrocytic markers (GFAP) in hippocampus. Scale bar, 40 μm (Iba-1), 25 μm (NeuN) and 20 μm (GFAP). (**B**) Iba1-stained hippocampal slices and highlighted regions from WT and PRL KO mice treated with either vehicle (top) or PLX3397 (bottom). Scale bar, 150 μm. (**C**) The number of Iba1$^+$ microglia. (**D**) Serum PRL concentrations in four groups. (**E**) Novel object recognition index. (**F**) Time to find the hidden platform in the Morris water maze (escape latency). (**G**) Time spent in the target quadrant in the Morris water maze probe trial (% total time in the target quadrant) for four groups. (**H**) Number of platform entries in probe trial. (**I**) Representative confocal images of NeuN (red) and Vglut1 (green). Scale bar, 80 μm. (**J-K**) Relative NeuN density and level of Vglut1 intensity. (**L-M**) Hippocampal synaptic density of WT and PRL KO mice were analyzed after 4 weeks treatment. Scale bar, 15 μm. (**N-Q**) Novel object recognition index (**N**), escape latencies (**O**), % total time in the target quadrant (**P**), number of platform entries in probe trial (**Q**) of microglial PRLR knockout mice and control mice were analyzed. (**R**) Representative confocal images of NeuN (red) and Vglut1 (green) in hippocampus. Scale bar, 80 μm. (**S-T**) Relative NeuN density and relative level of Vglut1 intensity. (**U-V**) Hippocampal synaptic density of microglial PRLR knockout mice and control mice. Scale bar, 15 μm. Data are presented as the mean ± SD. $n = 9$-10 mice/group (**D-H**, **N-Q**) and $n = 5$-6 mice/group (**C**, **J-M**, **S-V**). $^*p < 0.05$, $^{**}p < 0.01$, and $^{***}p < 0.001$; ns, not significant; unpaired two-tailed *t* test (**N**, **P-V**), two-way ANOVA (**F**, **O**) and one-way ANOVA (**C-E**, **G-M**)

activity of microglia toward synaptic elements. (Fig. 5C-D). Besides, phagocytic assay in vitro revealed that the engulfment of pHrodo green-conjugated synaptosomes was higher in PRL deficient primary microglia than control cells. PRL protein intervention could inhibit the increased engulfment of synaptosomes in PRL deficient primary microglia (Fig. 5E-F). Collectively, these vivo and vitro results indicated that PRL deficiency led to increased phagocytic ability of microglia, which may further result in the excessive elimination of synaptic structures.

To further examine whether enhanced microglial phagocytic capacity of synapses is a potential mechanism contributing to the harmful effects of PRL deficiency, mice were treated with minocycline. Minocycline, a microglial inhibitor, has been shown to affect microglial engulfment of synapses [44]. We found that PRL KO mice treated with minocycline showed attenuated cognitive impairment and synaptic loss, compared with saline-treated PRL KO mice (Fig. 5G-O). Furthermore, the abnormal increased microglial phagocytosis and excessive elimination of synaptic structures in vivo were restored in response to minocycline (Fig. 5P-S). Moreover, PRL KO primary microglia treated with minocycline displayed decreased phagocytic activity of synaptosomes compared to saline-treated control cells in vitro (Fig. 5T-U). These cumulative results suggested that PRL deficiency induced cognitive impairment and hippocampal synapse damage by increasing microglial phagocytic capacity of synapses.

Microglial PRLR knockout exaggerated cognitive dysfunction and hippocampal synaptic loss in HFD-diabetic mice

We next asked whether reduced PRL levels in diabetes influence cognitive performance and hippocampal synaptic density by modulating microglial synaptic phagocytosis. Microglial PRLR cKO mice and control mice were fed either a chow diet (CD) or a HFD (kcal%: fat, 60%; carbohydrate, 20%; protein, 20%) for 12 weeks. The performance of mice in behavioral tests was recorded. In comparison with CD mice, the cognition of HFD-diabetic mice was impaired. Microglial PRLR knockout exacerbated the cognitive impairment of HFD-diabetic mice, showing much less novel object preference, much longer time to reach the invisible platform, much less preference for the target quarter, and much fewer platform entries (Fig. 6A-D). Moreover, HFD-diabetic mice had decreased synapse density compared to CD mice, and microglial PRLR knockout exacerbated hippocampal synaptic loss in HFD-diabetic mice (Fig. 6E-I). Body weight recordings and tolerance tests showed that microglial PRLR knockout did not affect the body weight, glucose intolerance and insulin resistance of HFD-diabetic mice (Fig. S9A-C). These results suggested that the exacerbation of cognitive impairment and hippocampal synapse damage in microglial PRLR cKO diabetic mice was not associated with altered peripheral metabolic profiles.

Furthermore, we quantified the fluorescent signal of synaptic marker inside microglia by 3D reconstruction and surface rendering method. The results revealed that microglia in hippocampus of HFD-diabetic mice phagocytosed more synaptic structures, compared to CD mice, and this aberrant elimination of synaptic structures could be exacerbated by knockout of PRLR in microglia (Fig. 6J-K). Taken together, these data together suggested that microglial PRLR deficiency accelerated synaptic loss and cognitive declination in HFD-diabetic mice through excessive elimination of synaptic structures.

Microglial PRLR knockout promoted Rap1 activation by upregulating expression of RapGEFs, which in turn enhanced microglial phagocytic function in HFD-diabetic mice

Next, we explored how the blockade of PRL/PRLR signaling in microglia regulate the microglial phagocytic function in HFD-diabetic mice. Microglia isolated from microglial PRLR cKO mice and control mice (both fed by HFD) were subjected to RNA sequencing (RNA-seq) analysis (Fig. 7A). We identified 972 upregulated genes and 1139 downregulated genes in microglia from cKO/HFD mice compared to microglia from control/HFD mice (Fig. 7B). Differentially expressed genes (DEGs) from the two groups were analyzed by KEGG analyses.

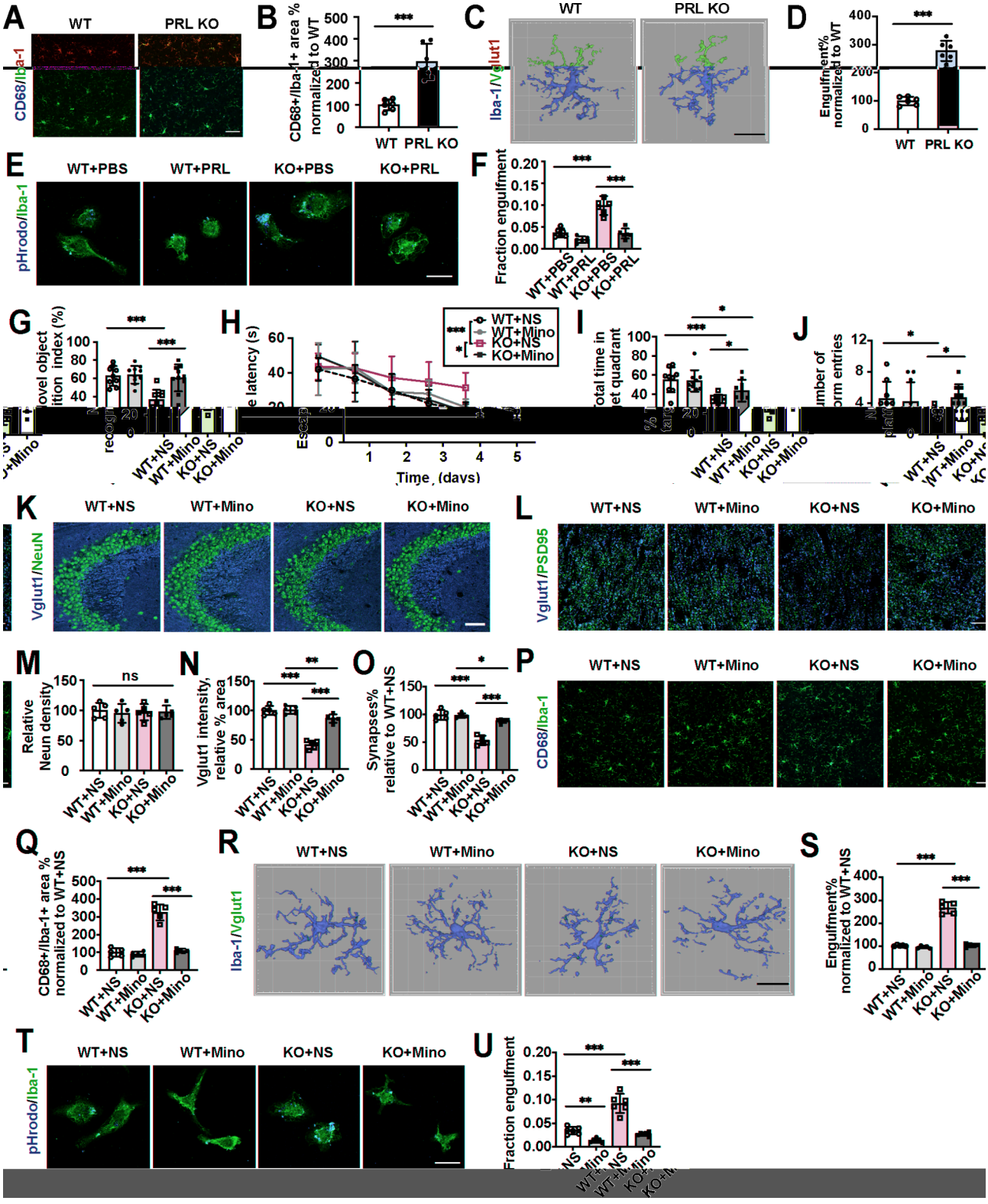

Fig. 5 (See legend on next page.)

(See figure on previous page.)

Fig. 5 PRL deficiency resulted in cognitive impairment and hippocampal synaptic damage by enhancing microglial phagocytic capacity of synapses. (**A**) Representative confocal images of Iba-1 (microglial marker, red) and lysosome marker (CD68, green) in the hippocampus. Scale bar, 45 μm. (**B**) Quantitation of fluoresce CD68/Iba-1. (**C-D**) Three-dimensional reconstruction and surface rendering demonstrate larger volumes of Vglut1 puncta inside Iba-1 positive microglia in hippocampus from PRL KO mice. Scale bar, 10 μm. (**E**) Representative images show that primary microglia (treated with PRL or PBS) phagocytosed pHrodo green-conjugated synaptosomes. Scale bar, 30 μm. $n = 6$ independent experiment. (**F**) Graph depicts the fraction of synaptosomes engulfed by microglia. (**G-J**) Novel object recognition index (**G**), escape latencies (**H**), % total time in the target quadrant (**I**), number of platform entries in probe trial (**J**) of four groups were analyzed. (**K**) Representative confocal images of NeuN (red) and Vglut1 (green) in hippocampus. Scale bar, 80 μm. (**L**) Representative confocal images of Vglut1 (green) and PSD95 (red) in hippocampus. Scale bar, 10 μm. (**M-N**) Relative NeuN density and Vglut1 intensity. (**O**) Synaptic density. (**P**) Representative confocal images of Iba-1and CD68 in the hippocampus. Scale bar, 45 μm. (**Q**) Quantitation of fluoresce CD68/Iba-1. (**R**) Three-dimensional surface rendering of immunostained Vglut1 (red) and Iba-1 (green) in hippocampus. Scale bar, 10 μm. (**S**) Engulfment of Vglut1$^+$ synapses by microglia. (**T**) Representative images show that primary microglia (treated with minocycline or saline) phagocytosed pHrodo green-conjugated synaptosomes. Scale bar, 30 μm. $n = 6$ independent experiment. (**U**) Graph depicts the fraction of synaptosomes engulfed by microglia. Data are presented as the mean ± SD. $n = 9$-10 mice/group (**G-J**) and $n = 5$-6 mice/group (**A-D**, **K-S**). *$p < 0.05$, **$p < 0.01$, and ***$p < 0.001$; ns, not significant; unpaired two-tailed *t* test (**A-D**), two-way ANOVA (**H**) and one-way ANOVA (**F-U**)

The top 10 upregulated KEGG pathways were mostly related to cell adhesion and reorganization of actin cytoskeleton, which are crucial for the phagocytic capacity of microglia (Fig. 7C). Cell adhesion and reorganization of the actin cytoskeleton were mainly modulated by the proteins of the small GTPase family, including the Rap subfamily, the Ras subfamily, the Rho subfamily, and so on [45]. We next performed gene set enrichment analyses (GSEA) and found that Rap1 signaling pathway (activated Rap1 interacts with multiple effector molecules) was significantly upregulated, suggesting an increase in Rap1 activation (Fig. 7D). The in vitro phagocytic assay showed that Rap1 inhibitor significantly weakened the effects of PRLR depletion on the microglial phagocytic ability to synaptosomes in HFD-diabetic mice, suggesting that knockout of PRLR enhanced microglial phagocytic function via increasing the activation of Rap1 (Fig. 7E-G).

The activation of Rap1 depends on its specific guanine nucleotide exchange factors (RapGEF1, RapGEF2, RapGEF3, RapGEF4, RapGEF5, and RapGEF6) [46]. To characterize the changes of RapGEFs in response to the knockout of PRLR, we analyzed the expression levels of RapGEFs in microglia from cKO/HFD mice and control/HFD mice. As shown in Fig. 7H, deletion of PRLR significantly increased the expression levels of RapGEF1, RapGEF3 and RapGEF4, while it did not influence the expression levels of other RapGEFs. We further confirmed the changes of RapGEFs in isolated microglia by qPCR (Fig. 7I). These results suggested that knockout of PRLR might increase the activation of Rap1 through upregulation of these three RapGEFs.

Infusion of PRL alleviated cognitive impairment and hippocampal synaptic damage in HFD-diabetic mice

To evaluate whether PRL infusion may be a potential strategy to attenuate diabetes-associated cognitive dysfunction, mice were implanted with a subcutaneous osmotic pump that delivered PRL to intracerebroventricular over a 4 week period through infusion cannula. As shown in Fig. S10A-C, the HFD-diabetic mice showed significant weight gain, and exhibited poorer glucose tolerance and insulin resistance compared to CD mice. PRL infusion reduced the body weight of HFD-diabetic mice and improved their glucose intolerance and insulin resistance, suggesting that PRL had beneficial effects in promoting metabolic health in diabetes. Moreover, continuous infusion of PRL in HFD-diabetic mice improved the performance of mice in behavioral tests and attenuated their hippocampal synaptic loss (Fig. 8A-I). Further examination of microglial engulfment of synapses indicated that continuous PRL infusion significantly reduced the number of synapses engulfed by microglia in hippocampus of the HFD-diabetic mice (Fig. 8.J-K). These results collectively indicated that PRL infusion could ameliorate the behavioral deficits and hippocampal pathology in HFD-diabetic mice via restoring the abnormal microglial phagocytosis of synapses.

Discussion

In this study, we revealed that PRL was associated with cognitive dysfunction and hippocampal damage in T2DM patients. We further revealed that in diabetes, a decrease in PRL levels triggered excessive microglia-mediated synapse engulfment, leading to hippocampal synaptic loss and cognitive dysfunction (Fig. 9). Notably, the restoration of PRL levels alleviated cognitive impairment and hippocampal synaptic damage in diabetic mice, suggesting a potential therapeutic approach for the promotion of cognitive health in diabetes.

Cognitive dysfunction is considered a vital comorbidity of T2DM, as diabetes not only increases the risk of MCI (OR: 1.44 [95% *CI* 1.35–1.53] and dementia (OR: 2.14 [95%*CI* 1.96–2.34]) but also accelerates the conversion from MCI to dementia (OR: 1.53 [95%*CI* 1.20–1.97]) [47, 48]. Hormones play a vital role in maintaining normal cognitive function [49]. It is widely acknowledged that peripheral hormones are involved in the regulation of cognitive function in individuals with diabetes [13–19]. However, studies on the relationship between pituitary hormones and altered cognitive function in individuals with diabetes are rare.

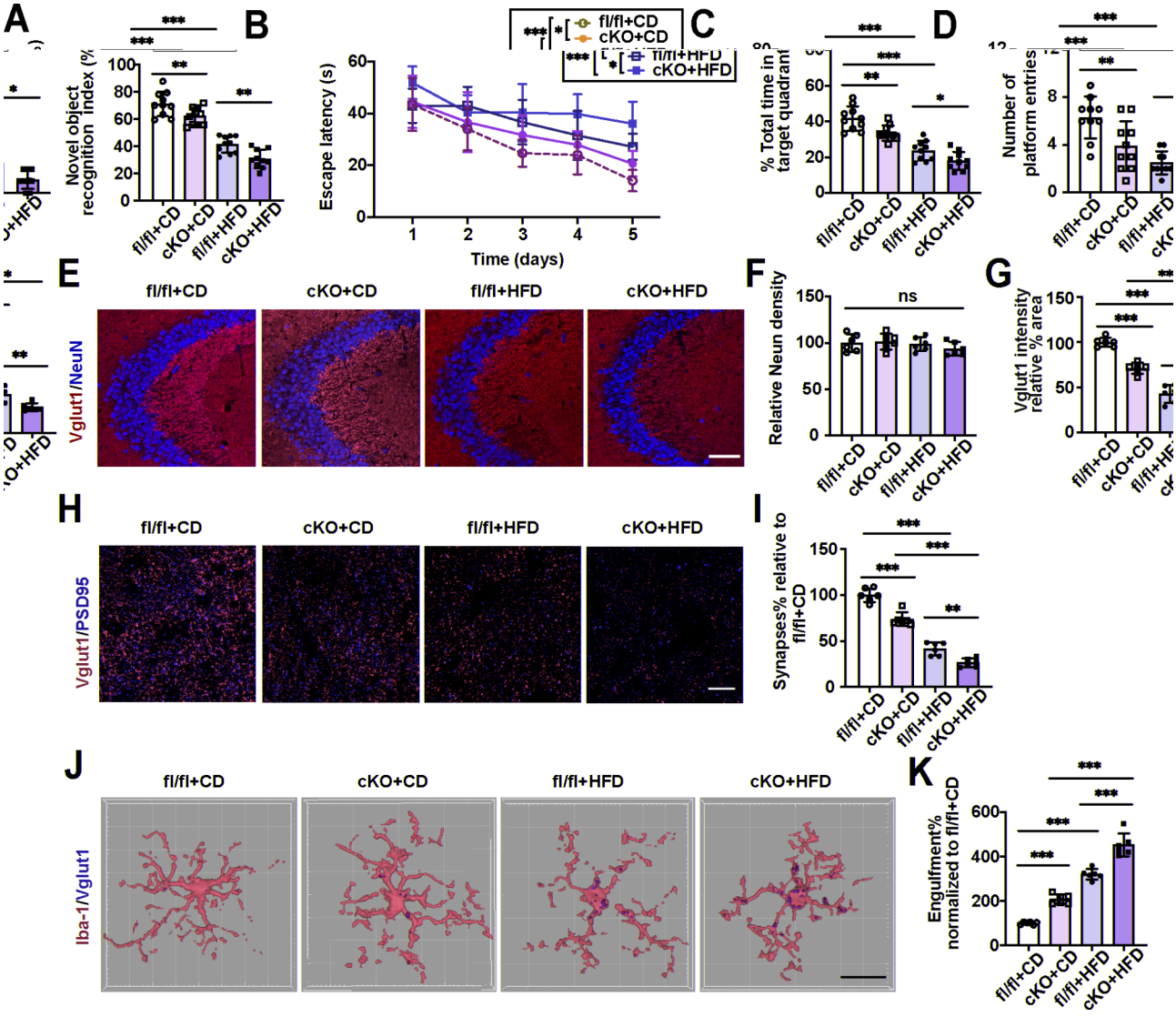

Fig. 6 Microglial PRLR knockout exacerbated the cognitive impairment and hippocampal synaptic loss in HFD-diabetic mice. (**A-D**) Novel object recognition index (**A**), escape latencies (**B**), % total time in the target quadrant (**C**), number of platform entries in probe trial (**D**) of four groups were analyzed. (**E**) Representative confocal images of NeuN (red) and Vglut1 (green) in hippocampus. Scale bar, 80 μm. (**F-G**) Relative NeuN density and relative level of Vglut1 intensity. (**H-I**) Hippocampal synaptic density in four groups. Scale bar, 15 μm. (**J**) Three-dimensional surface rendering of immunostained Vglut1 (red) and Iba-1 (green) in hippocampus of microglial PRLR knockout mice and control mice fed by CD or HFD. Scale bar, 10 μm. (**K**) Engulfment of $Vglut1^+$ synapses by microglia in four groups. Data are presented as the mean ± SD. $n = 10$ mice/group (**A-D**, **N-Q**) and $n = 6$ mice/group (**E-K**). $^*p < 0.05$, $^{**}p < 0.01$, and $^{***}p < 0.001$; ns, not significant; two-way ANOVA (**B**) and one-way ANOVA (**A**, **C-K**)

In the present study, we focused on the differences in pituitary hormone levels between cognitively healthy T2DM patients and T2DM patients with MCI, and we reported that T2DM patients with MCI had lower PRL levels. Logistic regression analyses demonstrated that among pituitary hormones, only a decrease in PRL level was significantly associated with the occurrence of MCI in patients with T2DM. Furthermore, compared with the fourth quartile, the first quartile of serum PRL levels was associated with a smaller hippocampus volume, suggesting an association between low PRL levels and decreased hippocampus volume in T2DM patients.

The hippocampus, a brain region important for maintaining cognitive function, is preferentially damaged in individuals with diabetes [50]. Synapses are the fundamental information-processing units necessary for hippocampal function. Synaptic damage and loss are central to hippocampal dysfunction, leading to cognitive decline, especially with respect to memory [7–9]. In various mouse models of diabetes, diabetic mice have been found to exhibit hippocampal synaptic loss, which was strongly correlated with cognitive decline [11, 51, 52]. In this study, we used an HFD-induced diabetic model, as mice subjected to an HFD not only dependably recapitulate

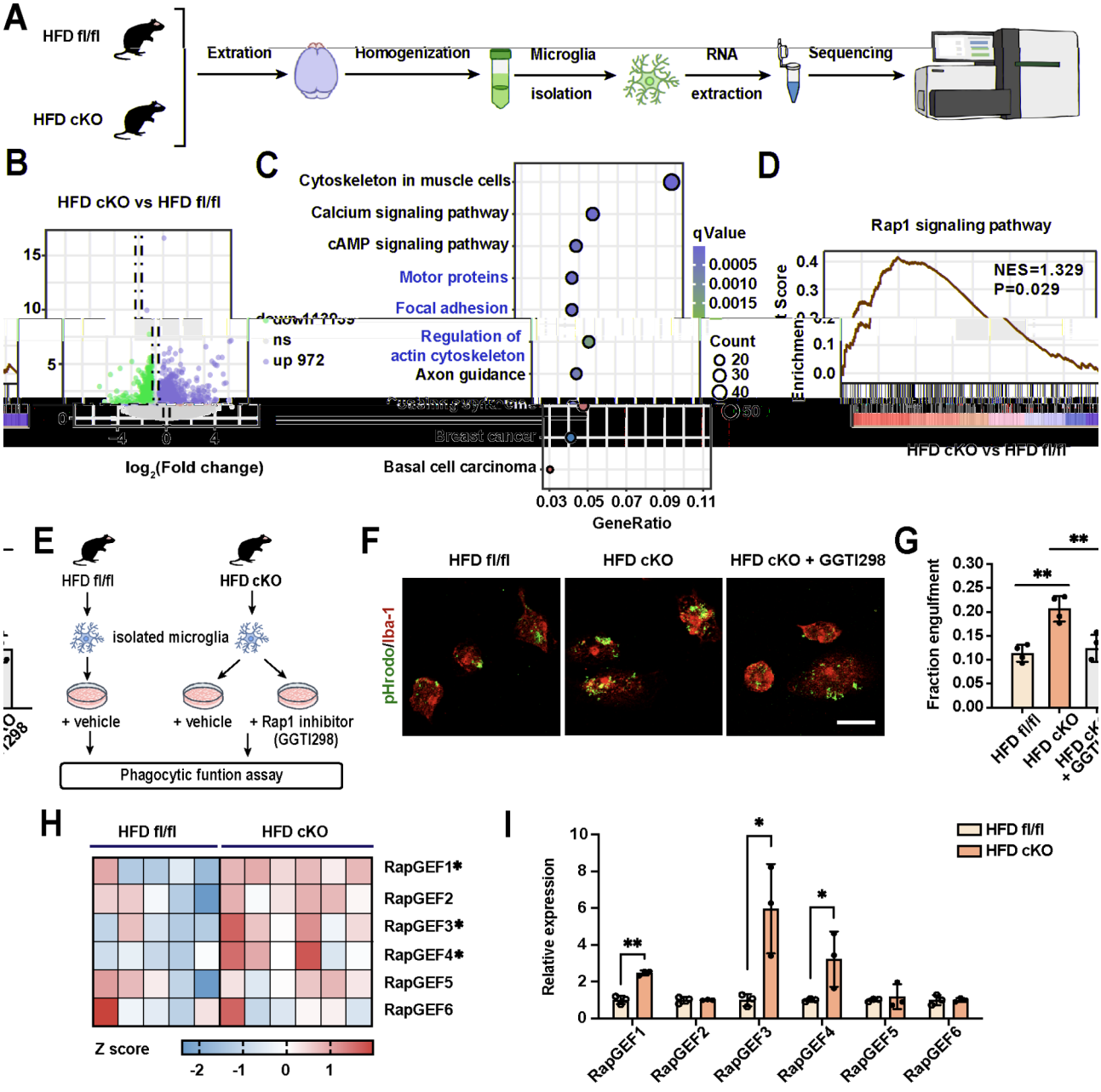

Fig. 7 Microglial PRLR knockout promoted Rap1 activation through upregulation of RapGEFs expression, which in turn enhanced the phagocytic function of microglia in HFD-diabetic mice. (**A**) Schematic for microglia isolation from adult mice, RNA extraction, RNA-seq, and bioinformatic analysis. (**B**) Volcano plot of DESeq2 analysis of microglia isolated from microglial PRLR knockout mice and control mice fed by HFD, using RNA-seq. (**C**) KEGG analysis of the 2,111 DEGs in these datasets. The top 10 upregulated KEGG pathways. (**D**) GSEA of DEGs in microglia of microglial PRLR knockout mice and control mice fed by HFD showing enrichment with upregulated gene sets in the Rap1 signaling pathway. (**E**) Schematic of cell experiments. (**F**) Representative images show that isolated microglia (treated with or without Rap1 inhibitor) phagocytosed pHrodo green-conjugated synaptosomes. Scale bar, 15 μm. (**G**) Graph depicts the fraction of synaptosomes engulfed by microglia. (**H**) Heatmap of Rap guanine nucleotide exchange factors (RapGEFs) in microglia. (**I**) qPCR assay to test the expression levels of RapGEFs in isolated microglial cells. Data are presented as the mean ± SD. $n = 5$-6 mice/group (**A-D**) and $n = 3$-4 mice/group (**E-I**). $^{*}p < 0.05$, $^{**}p < 0.01$, and $^{***}p < 0.001$; ns, not significant; unpaired two-tailed t test (**I**) and one-way ANOVA (**G**)

human T2DM conditions but also provide very good models for investigating the complications of T2DM [53]. Through dynamic diet intervention, we found that in diabetic mice, hippocampal synaptic loss occurred at the onset of cognitive impairment, while the number of hippocampal neurons did not change. Our findings indicate that hippocampal synaptic loss, rather than neuron loss, is the critical pathological feature of cognitive dysfunction at the early stage of diabetes. In addition, we also observed that a decrease in PRL level preceded the onset

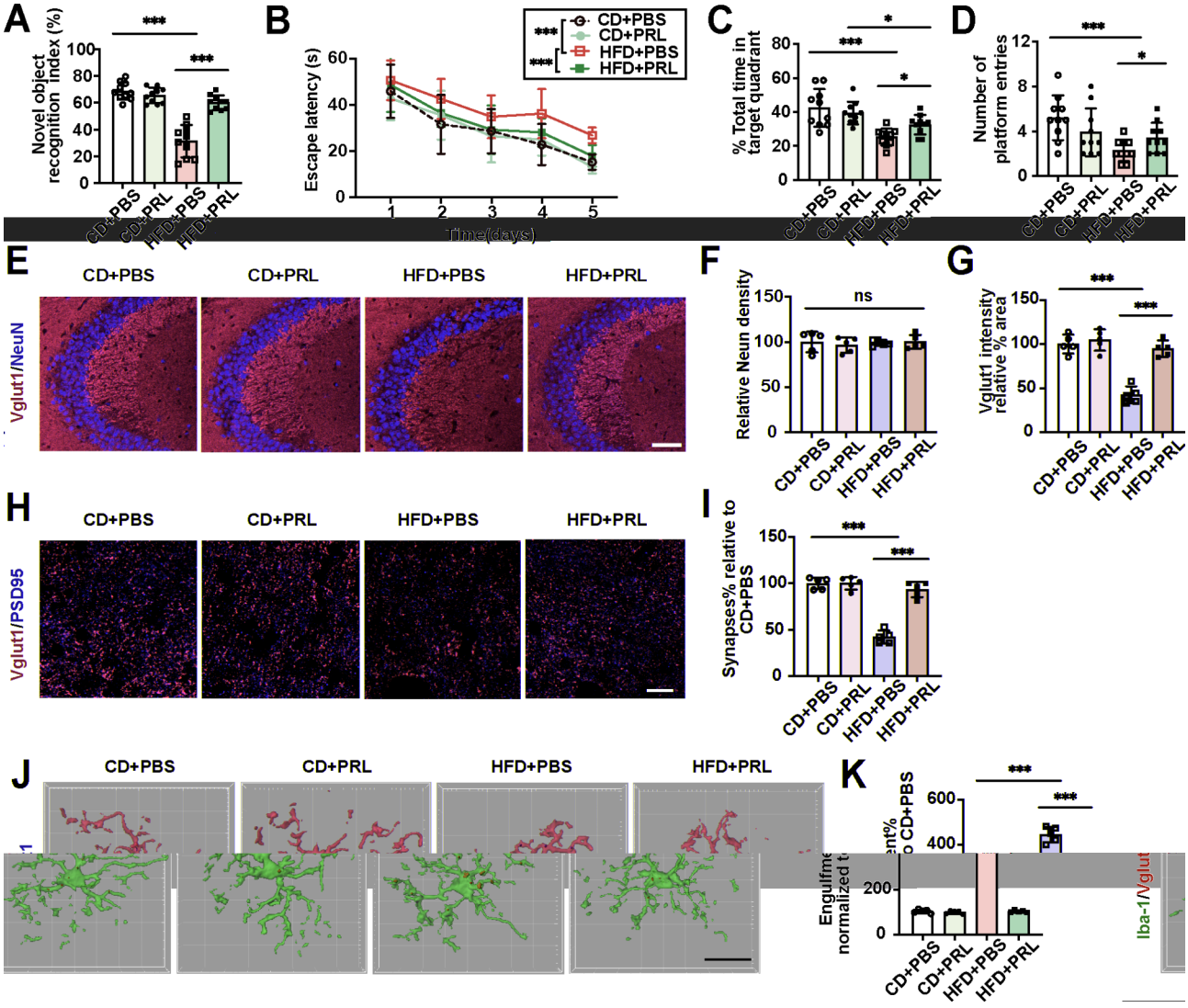

Fig. 8 Infusion of PRL improved cognitive impairment and hippocampal synaptic loss in HFD-diabetic mice. (**A-D**) Novel object recognition index (**A**), escape latencies (**B**), % total time in the target quadrant (**C**), number of platform entries in probe trial (**D**) of four groups were analyzed. (**E**) Representative confocal images of NeuN (red) and Vglut1 (green) in hippocampus. Scale bar, 80 μm. (**F-G**) Relative NeuN density and Vglut1 intensity. (**H-I**) Hippocampal synaptic density in four groups. Scale bar, 15 μm. (**J**) Three-dimensional surface rendering of immunostained Vglut1 (red) and Iba-1 (green) in hippocampus of CD mice and HFD-diabetic mice treated with PBS or PRL. Scale bar, 10 μm. (**K**) Engulfment of Vglut1$^+$ synapses by microglia in four groups. Data are presented as the mean ± SD. $n = 10$ mice/group (**A-D**, **N-Q**) and $n = 5$ mice/group (**E-K**). *$p < 0.05$, **$p < 0.01$, and ***$p < 0.001$; ns, not significant; two-way ANOVA (**B**) and one-way ANOVA (**A**, **C-K**)

of hippocampal synaptic loss and cognitive impairment in diabetic mice. Moreover, knockout of PRL directly reduced the number of synapses in the hippocampus and caused hippocampus-dependent cognitive impairment. Together, these results suggest that a decreased level of PRL is responsible for hippocampal synaptic loss and cognitive decline in diabetes. Importantly, a recent study demonstrated that diet-induced free fatty acid toxicity directly inhibited the synthesis and secretion of PRL by pituitary lactotrophs [54], which may account for the decreased level of PRL in HFD-induced diabetic mice.

The cell-specific mechanism underlying the effects of PRL level reduction on cognitive performance and hippocampal synaptic pathology was further studied. PRL actions are well known to be mediated by its receptor (PRLR) [38]. In the brain, PRLR is expressed in several regions, including the cerebral cortex, olfactory bulb, hypothalamus, hippocampus, amygdala, midbrain, etc [55]. At the cellular level, PRLR has been detected in hippocampal neurons [56], but whether PRLR is expressed in other hippocampal cell types is unclear. Our immunofluorescence assays in hippocampal tissue revealed that PRLR was expressed primarily in neurons and microglia,

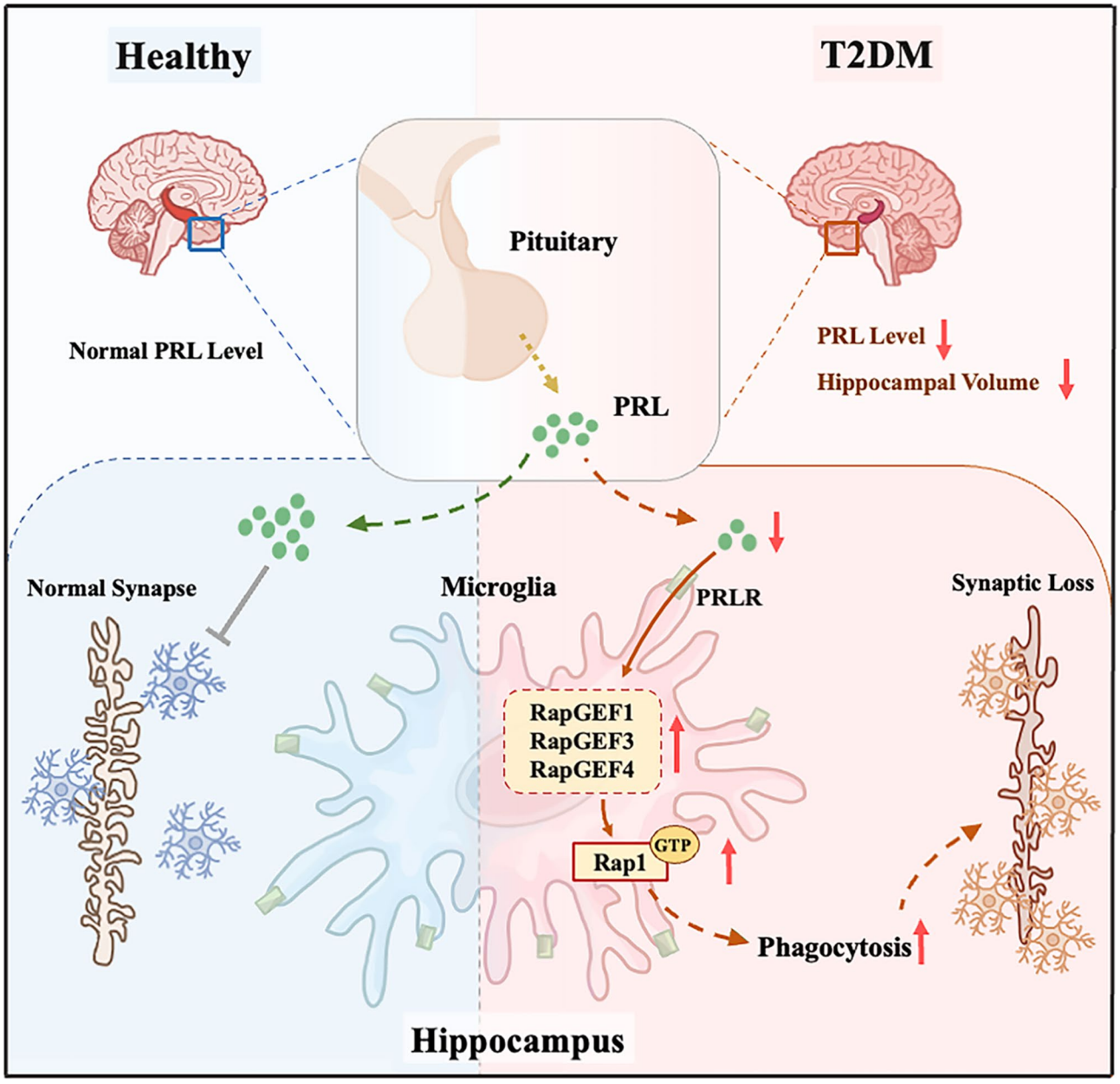

Fig. 9 Schematic showing that PRL deficiency drives diabetes-associated cognitive dysfunction by enhancing microglia-mediated synaptic engulfment. PRL modulates hippocampal synaptic density by regulating the microglial phagocytic ability to synapses for maintenance of normal cognitive function. In diabetes, PRL deficiency drives cognitive decline and hippocampal synaptic loss by enhancing microglial engulfment of synapses. Mechanistically, PRL diminishing promotes Rap1 activation by upregulating expression of RapGEFs, which in turn enhances microglial phagocytic ability

while PRLR was expressed at low levels in astrocytes. We also provided evidence that the specific knockout of PRLR in microglia, but not neurons, induced cognitive impairment and hippocampal synaptic loss. These results strongly support the role of microglia as mediators of the neurocognitive effects of PRL. As resident phagocytes in the central nervous system, microglia phagocytose damaged cells, debris, and excess and functionally weak synapses to maintain homeostasis in the brain [57, 58]. The abnormal phagocytic function of microglia results in excessive synaptic engulfment and subsequent synaptic loss [42]. Here, we found that PRL deficiency exacerbated microglial phagocytosis and triggered excessive microglia-mediated synapse engulfment. The inhibition of microglial phagocytic activity by minocycline weakened the elimination of synapses and rescued the cognitive deficits associated with hippocampal synaptic loss caused by PRL loss. Based on these findings, we determined that a decrease in PRL level had harmful effects on cognitive function and hippocampal synapse

density in diabetes by leading to an increase in microglial synaptic phagocytosis. Moreover, in diabetic mice, blocking PRL/PRLR signaling in microglia exacerbated the aberrant phagocytosis of synapses by microglia, further aggravating hippocampal synaptic loss and cognitive impairment. These results demonstrated that the decrease in PRL level in diabetes also drives hippocampal synaptic loss and cognitive decline by increasing microglial engulfment of synapses. Uncovering this mechanism contributes to identifying a specific therapeutic target for cognitive dysfunction in diabetic mice. While it is impossible to target only microglia in humans, a hormone receptor-specific and brain region-specific approach is possible. Treatments can preferentially target PRLR, and trial outcomes could focus on synapse degeneration in the hippocampus.

Additionally, we evaluated the potential of PRL intervention to treat cognitive dysfunction in diabetes. Our findings showed that PRL infusion therapy weakened microglia-mediated synapse elimination, restored hippocampal synaptic loss, and alleviated cognitive deficits in diabetic mice. These results suggest that PRL intervention is a promising therapeutic strategy to ameliorate diabetes-associated cognitive dysfunction. Notably, the infusion of PRL also decreased body weight and ameliorated glucose intolerance and insulin resistance in diabetic mice (Fig. S10A-C), suggesting that this therapeutic approach also has beneficial effects on peripheral metabolic organs.

Nevertheless, several limitations of this study should be noted. First, our clinical study is a cross-sectional study, which leads to potential for bias. Second, the exact mechanism by which the secretion of PRL is decreased in diabetes is not clear, and further investigation is needed. Third, 4% formaldehyde is the gold standard fixative for immunohistochemistry, which has limitations in detecting authentic signals of some molecules at the postsynapse. Other highly effective fixatives for immunostaining, such as glyoxal [59], should be tried in future experiments. Finally, intracerebroventricular infusion is a complicated procedure and may lead to brain damage. More research is needed to find a more precise and safer delivery system.

Conclusions

This study is the first to clarify that PRL is associated with the cognitive impairment and hippocampal damage in T2DM patients. Mechanistically, PRL deficiency enhancing microglia-mediated synapse elimination, ultimately leading to hippocampal synaptic loss and cognitive dysfunction in diabetes. Restoration of PRL could dampen the abnormal microglial phagocytosis of synapses, further ameliorating cognitive impairment and hippocampal damage in diabetic mice.

Abbreviations

T2DM	Type 2 diabetes mellitus
PRL	Prolactin
PRLR	Prolactin receptor
MCI	Mild cognitive impairment
PRLR	Prolactin receptor
TC	Total cholesterol
TG	Triglyceride
HDL-C	High density lipoprotein cholesterol
LDL-C	Low density lipoprotein cholesterol
HbA_{1c}	Glycated hemoglobin A1c
FSH	Follicle-stimulating hormone
LH	Luteinizing hormone
TSH	Thyroid stimulating hormone
ACTH	Adrenocorticotropic hormone
GH	Growth hormone
MMSE	Mini-Mental State Examination
MOCA	Montreal cognitive assessment
RBANS	Repeatable Battery for the Assessment of Neuropsychological Status
AAV	Adeno-associated virus
OF	Open field
NORT	Novel object recognition test
MWM	Morris water maze
GEF	Guanine nucleotide exchange factors

Supplementary Information

The online version contains supplementary material available at https://doi.org/10.1186/s12974-024-03289-z.

Supplementary Material 1

Supplementary Material 2

Supplementary Material 3

Acknowledgements

We are grateful to all study participants for their participation in the study.

Author contributions

J.J, Z.Z, J.W and Y.B designed the study. J.J, P.Z and Y.Y performed the study. X.X and T.W contributed to data analysis. J.J, P.Z and Y.Y wrote the draft of the paper. J.J, Z.Z, J.W and Y.B contributed to reviewing and revising the paper. J.J, P.Z and Y.Y share the first authorship. Since J.J contributed more effort (in designing research studies, conducting experiments, and analyzing data) than P.Z and Y.Y, J.J was listed first. Z.Z, J.W and Y.B are the corresponding authors. All authors read and approved the final version of the manuscript. All authors confirm that they had full access to all the data in the study and accept responsibility to submit the paper for publication.

Funding

This work was supported by grants from the National Natural Science Foundation of China Grant Award (No. 82470866, 82030026, 82450002, and 82470865), grants from the Natural Science Foundation of Jiangsu Province of China (BK20241721, BK20240116), and the funding for clinical trials from the affiliated Drum Tower Hospital, Medical School of Nanjing University (Grant No. 2022-LCYJ-PY-02 and 2022-LCYJ-ZD-03).

Data availability

No datasets were generated or analysed during the current study.

Declaration

Ethics approval and consent to participate

The study protocols of participants was approved by the ethics committee of Nanjing Drum Tower Hospital by the Ethics Review Committee of Nanjing Drum Tower Hospital Affiliated to Nanjing University Medical School (Approval number: 2017-017-01). All animal experimental procedures were conducted under the Institutional Animal Care and Use Committee-approved protocols

(2005010) at Nanjing University according to Laboratory Animal Care Guidelines.

Competing interests
The authors declare no competing interests.

Author details
[1]Department of Endocrinology, Endocrine and Metabolic Disease Medical Center, Affiliated Hospital of Medical School, Nanjing Drum Tower Hospital, Nanjing University, Nanjing, China
[2]Branch of National Clinical Research Centre for Metabolic Diseases, Nanjing, China

Received: 18 September 2024 / Accepted: 5 November 2024
Published online: 14 November 2024

References

1. Ahmad E, Lim S, Lamptey R, Webb DR, Davies MJ. Type 2 diabetes. Lancet. 2022;400:1803–20.
2. Zheng Y, Ley SH, Hu FB. Global aetiology and epidemiology of type 2 diabetes mellitus and its complications. Nat Rev Endocrinol. 2018;14:88–98.
3. Biessels GJ, Despa F. Cognitive decline and dementia in diabetes mellitus: mechanisms and clinical implications. Nat Rev Endocrinol. 2018;14:591–604.
4. Pearson-Stuttard J, Bennett J, Cheng YJ, Vamos EP, Cross AJ, Ezzati M, Gregg EW. Trends in predominant causes of death in individuals with and without diabetes in England from 2001 to 2018: an epidemiological analysis of linked primary care records. Lancet Diabetes Endocrinol. 2021;9:165–73.
5. van Sloten TT, Sedaghat S, Carnethon MR, Launer LJ, Stehouwer CDA. Cerebral microvascular complications of type 2 diabetes: stroke, cognitive dysfunction, and depression. Lancet Diabetes Endocrinol. 2020;8:325–36.
6. van Bussel FC, Backes WH, Hofman PA, van Oostenbrugge RJ, Kessels AG, van Boxtel MP, Schram MT, Stehouwer CD, Wildberger JE. Jansen JF.On the interplay of microvasculature, parenchyma, and memory in type 2 diabetes. Diabetes Care. 2015;38:876–82.
7. Qiu S, Hu Y, Huang Y, Gao T, Wang X, Wang D, Ren B, Shi X, Chen Y, Wang X, et al. Whole-brain spatial organization of hippocampal single-neuron projectomes. Science. 2024;383:eadj9198.
8. Koopmans F, van Nierop P, Andres-Alonso M, Byrnes A, Cijsouw T, Coba MP, Cornelisse LN, Farrell RJ, Goldschmidt HL, Howrigan DP, et al. SynGO: an Evidence-Based, Expert-Curated Knowledge Base for the synapse. Neuron. 2019;103:217–e234214.
9. Grünewald B, Wickel J, Hahn N, Rahmati V, Rupp H, Chung HY, Haselmann H, Strauss AS, Schmidl L, Hempel N, et al. Targeted rescue of synaptic plasticity improves cognitive decline in sepsis-associated encephalopathy. Mol Ther. 2024;32:2113–29.
10. Ni W, Niu Y, Cao S, Fan C, Fan J, Zhu L, Wang X. Intermittent hypoxia exacerbates anxiety in high-fat diet-induced diabetic mice by inhibiting TREM2-regulated IFNAR1 signaling. J Neuroinflammation. 2024;21:166.
11. Wang J, Li L, Zhang Z, Zhang X, Zhu Y, Zhang C, Bi Y. Extracellular vesicles mediate the communication of adipose tissue with brain and promote cognitive impairment associated with insulin resistance. Cell Metab. 2022;34:1264–e12791268.
12. Südhof TC. Towards an understanding of synapse formation. Neuron. 2018;100:276–93.
13. Launer LJ. Interrelationships among central insulin signalling, diabetes, and cognitive impairment. Lancet Neurol. 2020;19:640–2.
14. Lee CC, Huang CC, Hsu KS. Insulin promotes dendritic spine and synapse formation by the PI3K/Akt/mTOR and Rac1 signaling pathways. Neuropharmacology. 2011;61:867–79.
15. Irving A, Harvey J. Regulation of hippocampal synaptic function by the metabolic hormone leptin: implications for health and disease. Prog Lipid Res. 2021;82:101098.
16. Pathak NM, Pathak V, Gault VA, McClean S, Irwin N, Flatt PR. Novel dual incretin agonist peptide with antidiabetic and neuroprotective potential. Biochem Pharmacol. 2018;155:264–74.
17. Batista AF, Forny-Germano L, Clarke JR, Lyra ESNM, Brito-Moreira J, Boehnke SE, Winterborn A, Coe BC, Lablans A, Vital JF, et al. The diabetes drug liraglutide reverses cognitive impairment in mice and attenuates insulin receptor and synaptic pathology in a non-human primate model of Alzheimer's disease. J Pathol. 2018;245:85–100.
18. Byun YG, Kim NS, Kim G, Jeon YS, Choi JB, Park CW, Kim K, Jang H, Kim J, Kim E, et al. Stress induces behavioral abnormalities by increasing expression of phagocytic receptor MERTK in astrocytes to promote synapse phagocytosis. Immunity. 2023;56:2105–e21202113.
19. Nie R, Lu J, Xu R, Yang J, Shen X, Ouyang X, Zhu D, Huang Y, Zhao T, Zhao X, et al. Ipriflavone as a non-steroidal glucocorticoid receptor antagonist ameliorates diabetic cognitive impairment in mice. Aging Cell. 2022;21:e13572.
20. Gao X, Sun H, Wei Y, Niu J, Hao S, Sun H, Tang G, Qi C, Ge J. Protective effect of melatonin against metabolic disorders and neuropsychiatric injuries in type 2 diabetes mellitus mice. Phytomedicine. 2024;131:155805.
21. Zaidi M, Yuen T, Kim SM. Pituitary crosstalk with bone, adipose tissue and brain. Nat Rev Endocrinol. 2023;19:708–21.
22. Martínez-Moreno CG. Arámburo C.Growth hormone (GH) and synaptogenesis. Vitam Horm. 2020;114:91–123.
23. Luan S, Bi W, Shi S, Peng L, Li Z, Jiang J, Gao L, Du Y, Hou X, He Z, Zhao J. Thyrotropin receptor signaling deficiency impairs spatial learning and memory in mice. J Endocrinol. 2020;246:41–55.
24. Xiong J, Kang SS, Wang Z, Liu X, Kuo TC, Korkmaz F, Padilla A, Miyashita S, Chan P, Zhang Z, et al. FSH blockade improves cognition in mice with Alzheimer's disease. Nature. 2022;603:470–6.
25. Carretero J, Sánchez-Robledo V, Carretero-Hernández M, Catalano-Iniesta L, García-Barrado MJ, Iglesias-Osma MC. Blanco EJ.Prolactin system in the hippocampus. Cell Tissue Res. 2019;375:193–9.
26. ElSayed NA, Aleppo G, Aroda VR, Bannuru RR, Brown FM, Bruemmer D, Collins BS, Hilliard ME, Isaacs D, Johnson EL, et al. 2. Classification and diagnosis of diabetes: standards of Care in Diabetes-2023. Diabetes Care. 2023;46:S19–40.
27. Arevalo-Rodriguez I, Smailagic N, Roqué-Figuls M, Ciapponi A, Sanchez-Perez E, Giannakou A, Pedraza OL, Bonfill Cosp X, Cullum S. Mini-mental State Examination (MMSE) for the early detection of dementia in people with mild cognitive impairment (MCI). Cochrane Database Syst Rev. 2021;7:Cd010783.
28. Davis DH, Creavin ST, Yip JL, Noel-Storr AH, Brayne C, Cullum S. Montreal Cognitive Assessment for the detection of dementia. Cochrane Database Syst Rev. 2021;7:Cd010775.
29. Langa KM, Levine DA. The diagnosis and management of mild cognitive impairment: a clinical review. JAMA. 2014;312:2551–61.
30. Cheng Y, Wu W, Wang J, Feng W, Wu X, Li C. Reliability and validity of the repeatable battery for the Assessment of Neuropsychological Status in community-dwelling elderly. Arch Med Sci. 2011;7:850–7.
31. Płotek W, Łyskawa W, Kluzik A, Grześkowiak M, Podlewski R, Żaba Z, Drobnik L. Evaluation of the trail making test and interval timing as measures of cognition in healthy adults: comparisons by age, education, and gender. Med Sci Monit. 2014;20:173–81.
32. Freund MC, Bugg JM, Braver TSA. Representational Similarity Analysis of Cognitive Control during Color-Word Stroop. J Neurosci. 2021;41:7388–402.
33. Stanford SC. The Open Field Test: reinventing the wheel. J Psychopharmacol. 2007;21:134–5.
34. Leger M, Quiedeville A, Bouet V, Haelewyn B, Boulouard M, Schumann-Bard P. Freret T.Object recognition test in mice. Nat Protoc. 2013;8:2531–7.
35. Yamamoto M, Guo DH, Hernandez CM, Stranahan AM. Endothelial Adora2a activation promotes blood-brain barrier breakdown and cognitive impairment in mice with Diet-Induced insulin resistance. J Neurosci. 2019;39:4179–92.
36. Xiao F, Xia T, Lv Z, Zhang Q, Xiao Y, Yu J, Liu H, Deng J, Guo Y, Wang C, et al. Central prolactin receptors (PRLRs) regulate hepatic insulin sensitivity in mice via signal transducer and activator of transcription 5 (STAT5) and the vagus nerve. Diabetologia. 2014;57:2136–44.
37. Beyene J, Atenafu EG, Hamid JS, To T, Sung L. Determining relative importance of variables in developing and validating predictive models. BMC Med Res Methodol. 2009;9:64.
38. Bernard V, Young J, Chanson P, Binart N. New insights in prolactin: pathological implications. Nat Rev Endocrinol. 2015;11:265–75.
39. Elmore MR, Najafi AR, Koike MA, Dagher NN, Spangenberg EE, Rice RA, Kitazawa M, Matusow B, Nguyen H, West BL. Green KN.Colony-stimulating factor 1 receptor signaling is necessary for microglia viability, unmasking a microglia progenitor cell in the adult brain. Neuron. 2014;82:380–97.
40. Csikós V, Oláh S, Dóra F, Arrasz N, Cservenák M. Dobolyi A.Microglia depletion prevents lactation by inhibition of prolactin secretion. iScience. 2023;26:106264.
41. Wolf SA, Boddeke HW, Kettenmann H. Microglia in Physiology and Disease. Annu Rev Physiol. 2017;79:619–43.

42. Ding X, Wang J, Huang M, Chen Z, Liu J, Zhang Q, Zhang C, Xiang Y, Zen K, Li L. Loss of microglial SIRPα promotes synaptic pruning in preclinical models of neurodegeneration. Nat Commun 2021, 12:2030.
43. Taddei RN, Perbet R, Mate de Gerando A, Wiedmer AE, Sanchez-Mico M, Connors Stewart T, Gaona A, Melloni A, Amaral AC, Duff K, et al. Tau oligomer-containing synapse elimination by microglia and astrocytes in Alzheimer Disease. JAMA Neurol. 2023;80:1209–21.
44. Li X, Hu B, Guan X, Wang Z, Zhou Y, Sun H, Zhang X, Li Y, Huang X, Zhao Y, et al. Minocycline protects against microgliopathy in a Csf1r haplo-insufficient mouse model of adult-onset leukoencephalopathy with axonal spheroids and pigmented glia (ALSP). J Neuroinflammation. 2023;20:134.
45. Körber S, Junemann A, Litschko C, Winterhoff M, Faix J. Convergence of ras- and rac-regulated formin pathways is pivotal for phagosome formation and particle uptake in Dictyostelium. Proc Natl Acad Sci U S A. 2023;120:e2220825120.
46. Jaśkiewicz A, Pająk B, Orzechowski A. The many faces of Rap1 GTPase. Int J Mol Sci 2018, 19.
47. Jia L, Du Y, Chu L, Zhang Z, Li F, Lyu D, Li Y, Li Y, Zhu M, Jiao H, et al. Prevalence, risk factors, and management of dementia and mild cognitive impairment in adults aged 60 years or older in China: a cross-sectional study. Lancet Public Health. 2020;5:e661–71.
48. Biessels GJ, Nobili F, Teunissen CE, Simó R. Scheltens P.Understanding multifactorial brain changes in type 2 diabetes: a biomarker perspective. Lancet Neurol. 2020;19:699–710.
49. Calsolaro V, Bottari M, Coppini G, Lemmi B. Monzani F.Endocrine dysfunction and cognitive impairment. Minerva Endocrinol (Torino). 2021;46:335–49.
50. Hempel R, Onopa R, Convit A. Type 2 diabetes affects hippocampus volume differentially in men and women. Diabetes Metab Res Rev. 2012;28:76–83.
51. Li Q, Zhao Y, Guo H, Li Q, Yan C, Li Y, He S, Wang N, Wang Q. Impaired lipophagy induced-microglial lipid droplets accumulation contributes to the buildup of TREM1 in diabetes-associated cognitive impairment. Autophagy. 2023;19:2639–56.
52. Jiang T, Li Y, He S, Huang N, Du M, Zhai Q, Pu K, Wu M, Yan C, Ma Z. Wang Q.Reprogramming astrocytic NDRG2/NF-κB/C3 signaling restores the diabetes-associated cognitive dysfunction. EBioMedicine. 2023;93:104653.
53. Heydemann AA. Overview of Murine High Fat Diet as a Model for Type 2 Diabetes Mellitus. J Diabetes Res 2016, 2016:2902351.
54. Ji X, Yin H, Gu T, Xu H, Fang D, Wang K, Sun H, Tian S, Wu T, Nie Y, et al. Excessive free fatty acid sensing in pituitary lactotrophs elicits steatotic liver disease by decreasing prolactin levels. Cell Rep. 2024;43:114465.
55. Cabrera-Reyes EA, Limón-Morales O, Rivero-Segura NA, Camacho-Arroyo I. Cerbón M.Prolactin function and putative expression in the brain. Endocrine. 2017;57:199–213.
56. Costa-Brito AR, Gonçalves I, Santos CRA. The brain as a source and a target of prolactin in mammals. Neural Regen Res. 2022;17:1695–702.
57. Prinz M, Jung S, Priller JM, Biology. One Century Evol Concepts Cell. 2019;179:292–311.
58. Madore C, Yin Z, Leibowitz J, Butovsky O. Microglia, lifestyle stress, and Neurodegeneration. Immunity. 2020;52:222–40.
59. Konno K, Yamasaki M, Miyazaki T, Watanabe M. Glyoxal fixation: an approach to solve immunohistochemical problem in neuroscience research. Sci Adv. 2023;9:eadf7084.

Publisher's note

Springer Nature remains neutral with regard to jurisdictional claims in published maps and institutional affiliations.